PFC/RR-88-15 DOE/ET-51013260

SAFETY AND PROTECTION FOR LARGE-SCALE MAGNET SYSTEMS – FY88 REPORT

R.J. Thome, M. Zimmermann, M. Kazimi, N. Siu, M. Oshima
A.M. Dawson, General Editor

December 1988

Plasma Fusion Center
Massachusetts Institute of Technology
Cambridge, Massachusetts 02139

Submitted to
Idaho National Engineering Laboratory
Idaho Falls, Idaho

Table of Contents

Table of Contents, cont.

List of Figures

List of Figures, cont.

List of Tables

1.0 Introduction

The large magnet safety and protection effort this past year focussed on two areas: the preliminary analysis of fault conditions for fusion magnet systems and the initial development of a transportable, safety-oriented code for study of quench characteristics in large magnets.

Section 2.0 presents the results of an assessment of electrical failure consequences in a PF magnet system on the loads experienced by the PF and TF magnets. After a general discussion of the manner in which the PF system is coupled to other reactor subsystems, two types of faults on PF coils were selected for evaluation: short circuits across the terminals and control system faults which lead to continued coil charging at maximum power supply voltage. The study is done using a simplified model based on the characteristics of the Compact Ignition Tokamak (major radius=2.1 m). These coils are liquid-nitrogen cooled, but resistive in nature and would be expected to behave somewhat differently than comparable superconducting coils.

It was found that the types of short circuits studied do not pose large risks provided reasonable design margins for fault-related structural overload are assumed to be used. The overloads are of order two, hence the structure must be capable of withstanding loads of this level, but not in the course of normal, repeated operation. Voltage-driven faults were found to be more severe, in that some form of protective action will be required to keep overloads on selected PF coils and on the TF (out-of-plane) within the selected factor of two relative to normal operation. In all cases the time scale for protective reaction was considered to be feasible. Three different types of plasma disruption were considered, but all were roughly equivalent in their overall impact on the load multiplication factors during faults. The list of fault conditions considered was not exhaustive, but results are encouraging provided that the assumed factor of two for structural overload in case of fault is realistic. Further consideration, extending the list of possible faults is necessary as the design evolves.

Section 3.0 presents the status of the initial development of a transportable code for safety-oriented quench analysis. Modification of an existing stability code for internally cooled superconductors has begun. Sample cases have been run and alterations have been incorporated which will allow protective action to be taken.

Problems associated with time scale have been addressed in a preliminary fashion. This involves the fact that stability and recovery (or nonrecovery) relative to a disturbance for a conductor of this type occurs on the time scale of 1-10 ms whereas global parameters associated with quench, protection, and safety occur on the time scale of tens of seconds to minutes in large magnets. Further work with respect to code efficiency is required to allow cases to be run with reasonable cpu time expenditure. We have also begun to address the issue of voltage distribution within a quenching coil since we consider this to be an important source for potential failure initiation. Further development of this code will be performed in the coming fiscal year.

2.0 THE CONSEQUENCES OF ELECTRICAL FAILURES in PF MAGNET SYSTEMS FOR TOKAMAKS

M. ZIMMERMANN, M.S. KAZIMI, N.O. SIU, and R.J. THOME

2.1 Introduction

Failure consequences must be analysed to perform a risk and reliability analysis of magnet systems. The consequences of two groups of electrical faults which originate in the poloidal field (PF) coil system, shorts between coil terminals and faults with constant applied voltage, have been investigated by using a simplified model of the Compact Ignition Tokamak. It was found that shorts do not pose large risks.However, under selected scenarios with constant applied voltage, the out-of-plane forces at the inner corner of the toroidal field (TF) magnets were found to increase substantially. For all scenarios, the type of plasma disruption had modest impact on the force distributions for the PF and TF magnets.

The design of magnet systems for fusion devices, such as the Compact Ignition Tokamak (CIT) in the United States and the Next European Torus (NET) in Europe involves considerable uncertainties about development and operation costs, system performance,availability and safety considerations. Decisions made during the early design phases may have a large impact on performance, costs and schedules and should therefore be based upon, and reviewed in light of the overall system performance perspective.

While earlier design studies such as the International Tokamak Reactor Study (INTOR)[1] have been concerned principally with achieving engineering objectives, near-term and currently operating devices such as the Tokamak Fusion Test Reactor (TFTR)[2] are now emphasizing reliability programs and physics gains. In addition, the NET project has adopted a reliability and availablility assurance program from its very beginning[3]. A generic framework for a design concept for fusion reactors that includes safety and reliability considerations has also been developed[4] and was proposed and expanded for an integrated risk-based design objective for CIT[5]. All these fusion studies have emphasized that magnet systems remain a major concern in terms of system availability, costs and safety of fusion devices. This is due to their high development costs, the large amounts of energy stored in the coils during operation, and the long downtimes and high costs that are associated with repairs or replacement of magnets. This makes the design of highly reliable magnet systems mandatory.

Up to now, the development of fault trees and consequence analysis has been primarily directed towards the toroidal field (TF) coil system[6]. The PF coil system has been considered as having a similar fault tree structure. While this is certainly true for most of the coil structures and cooling system, the operational characteristics and requirements of the PF coil system are different due to the pulsed operation and more diversified operational tasks of the PF systems. Additionally, very little published work on fault analysis such as that for TFTR[7] exists, and the database on fault consequences is still small, as recent surveys have shown[8]. Thus, the impact of the PF coil system on the overall magnet system and other reactor components was investigated and an analysis of failures and fault consequences for faults originating in the PF power supply and control system has been performed.

2.2 A RELIABILITY ASSESSMENT STRATEGY

The outlined strategy is based on fault tree methodology that allows one to integrate availability and consequence analysis in a common framework for systems with a gradually developing database such as magnet systems. The fault tree for the magnet system was divided into one for the TF coil and one for each component of the PF coil system. These fault trees were structured in two basic parts:

1. a top part, which has the overall top event "unavailability of the magnet system" (similar to the NET study[3,6]) and that contains only failure modes that are defined in terms of the "unavailability" of a subsystem or component, and
2. a bottom part, extending from the lowest level of failure of the top tree down to the basic failure modes of each subsystem or component. The failure modes in this tree are described in terms of physical failures. By using this structure, the top part will only contain "OR"-gates since the failure of a single subsystem will cause the complete system to fail. Also, this part will require only minor modifications to be widely applicable to most magnet systems. The NET reliability assessment[6] has already been found to provide most of the top part of the fault tree for the TF coil system.

The bottom part is more specific and different for each design when followed to the lowest level of failure.

The interface between the top and bottom of the fault tree also provides the basis for the consequence analysis and lists the initiating events. An event tree analysis can then be performed starting from each initiating event. The effective number of initiating events can be reduced when events with similar consequences are grouped together. Finally the consequences can be grouped into several levels of severity, where lower severity levels only affect the plant availability while the higher levels are safety related. Thus, downtimes as well as safety risks can be assessed in a single framework[10].

However, the current database[1,3,6,9] only permits drawing these fault trees on a generic basis for the TF coil system[10]. Parts of these trees, such as those for the coils and the cooling system, can be transferred to the PF coil system, but the PF power supply and Protection, Instrumentation and Control (PIC) system need more analysis. This is of particular importance since a large number of TF coil system basic failure modes are related to interactions with the PF coils.

2.3 INTERACTIONS OF THE PF COIL SYSTEM WITH OTHER SYSTEMS

The PF coil system is responsible for initiating and providing the plasma current and for building up and controlling the position and shape of the plasma. This makes the pulsed operation of the PF coils necessary as each coil will usually follow a different current scenario.

The concept of a Fault Interaction Matrix[2,9] has been adopted here, since it allows identification of the coupling between systems. Such a matrix has been developed for the PF coil system and is shown in Table 2.1. It describes the impact of each PF coil subsystem listed in the top row of the table on each of the systems listed in the left column. The table includes interactions that occur during normal operation and under fault conditions. It can be seen that only a few system pairs have no considerable impact on each other, which demonstrates the intense coupling that is related to the PF coil subsystems. Most of this coupling is due to the pulsed operation and the strong impact and reliance on feedback information from the plasma. This requires a complex Protection, Instrumentation and Control (PIC) system, that uses feedback and preprogrammed control and sets controls on different time scales as necessary. Clearly, this complexity also leaves a large potential for fault initiation.

2.4 THE POLOIDAL FIELD POWER SUPPLY AND CONTROL SYSTEM

The detailed designs of the PF power supply and PIC system differ in various fusion devices but a review of the designs used for the Tokamak Fusion Test Reactor (TFTR)[10,11] and the Joint European Torus (JET)[12] provide the basic design and operation features for these systems[6]. It can be assumed that devices of the next generation such as the Compact Ignition Tokamak (CIT) and the Next European Torus (NET) will use similar

Table 2.1. Fault Interaction Matrix for the Poloidal Field (PF) Coil System

Fault Interaction Matrix for PF Magnet System				
	Poloidal Field Coils System	Poloidal Field Coils Cooling System	Poloidal Field Power Supply System	Poloidal Field PIC System
PF Coils System	EM,M,T	T	E,P	M,E,P,C
PF Cooling System	EM,M	-	E	P,C
PF Power Supply System	EM,M	E	E	C
PF PIC System	EM,M	E	E	E,C
TF Magnet System	EM,M	T	E,P	P,C
First Wall, Blanket, and Limiter System	EM,M,P	-	P	P
Vacuum Vessel and Shield	EM,M	-	P	P
Divertor System	EM,M	-	P	P,C
Cryogenics Cooling System and Cryostat	EM,M	M,T	P	P
Intermediate Cooling Cycles	EM,M	-	-	-
Plasma Heating System	EM,M	-	E,P	P,C
Plasma Fueling System	M	-	P	P,C
Plant Power Supply	EM	E	E	E,P
Central Plant PIC System	EM	E	P	E,P

EM: electromagnetic interaction, e.g. via eddy currents or electromagnetic force

M: mechanical interaction, e.g. via common support structure

T: thermal coupling, e.g. common cooling media

E: electrical interaction, e.g. coupling via busbars or shorts from intermittent connections

P: plasma interaction, e.g plasma disruptions

C: Control errors, e.g. control system malfunctioning or operator errors

designs. In general, the PF coils external to the TF coils are controlled on a slow time scale and are mainly operated with preprogrammed currents, while the coils inside the TF coils (which will be referred to as internal or IC coils here) are controlled both actively and rapidly. For the following discussion it is assumed that all coil-pair power supplies provide unidirectional voltages, and mechanical reversing switches are used to allow for bidirectional outputs. Such a circuit with independent unidirectional power supplies is under discussion for CIT. It is economically acceptable and reduces the circuit complexity considerably. The output current of the power supplies will be checked periodically and a ground fault detection system will sense currents to ground. When a ground fault is detected, a crowbar switch will be closed so that the coils will be connected to ground and discharged. A switching network that includes a circuit breaker, mechanical reversing switches and possibly a forced commutated circuit with resistors will produce the voltage

for the coil terminals. Clock signals are provided by a master clock system, which receives the waveform breakpoint information from a waveform generator in a high-level control system. The coils of each mirror coil pair are assumed to be connected in series.

2.5 FAULT SCENARIOS FOR THE PF POWER SUPPLY AND PIC SYSTEM

The PF coils, power supply and PIC system have been analyzed for potential electrical failures. This analysis has revealed that a large number of failures may be grouped in two basic categories:

1. electrical shorts, where a pair or a single PF coil is shorted across terminals, between turns or to ground, and,
2. erroneous control or switching, where coils are accidentally driven with a voltage that does not produce the desired preprogrammed currents.

The design of the CIT machine with a mean radius of 2.1 m[8] was taken as a reference for this study. The CIT configuration includes 7 external PF coils, where 3 coils, PF1 to PF3, comprise the central solenoid, PF4 and PF5 are located at the top of the TF coil, and PF6 and PF7 are located along the outer leg of the TF coil. The location of these coils is indicated in Fig. 2.5.1. Coils PF1 to PF3 are the main ohmic heating coils, and PF4 and PF7 provide the basic plasma shaping. There are also 3 IC coils which will be actively controlled on a short time scale. All coils are made of copper or copper/Inconel laminate and are liquid-nitrogen cooled. The maximum magnetic field at 2.1 m will be 11 T and the maximum plasma current that is held for 5 s, is 11 MA. One complete pulse takes 28.26 s and the coils are heated adiabatically during the pulse and cooled down to LN_2 temperature between pulses.

The fault scenarios have been analyzed to investigate the potential for violating three design factors:

1. forces and stresses in the external PF coils and the out-of-plane loads on the TF coils should be kept within a chosen multiple of the maximum values that will be obtained under normal operation conditions,
2. unanticipated force reversals are to be avoided, and
3. the maximum temperature in any coil should not exceed a selected temperature.

Because the plasma behavior depends strongly on the PF coil current scenario, any disturbance quickly leads to a plasma disruption. Thus, a plasma disruption will follow a major fault and three types of disruptions have been considered here:

1. a plasma disruption with stationary plasma and a plasma current breakdown of $-1\ MA/ms$,
2. a horizontal disruption, occurring within 5 ms, and
3. a vertical disruption which reduces the plasma current to zero within 210 ms.

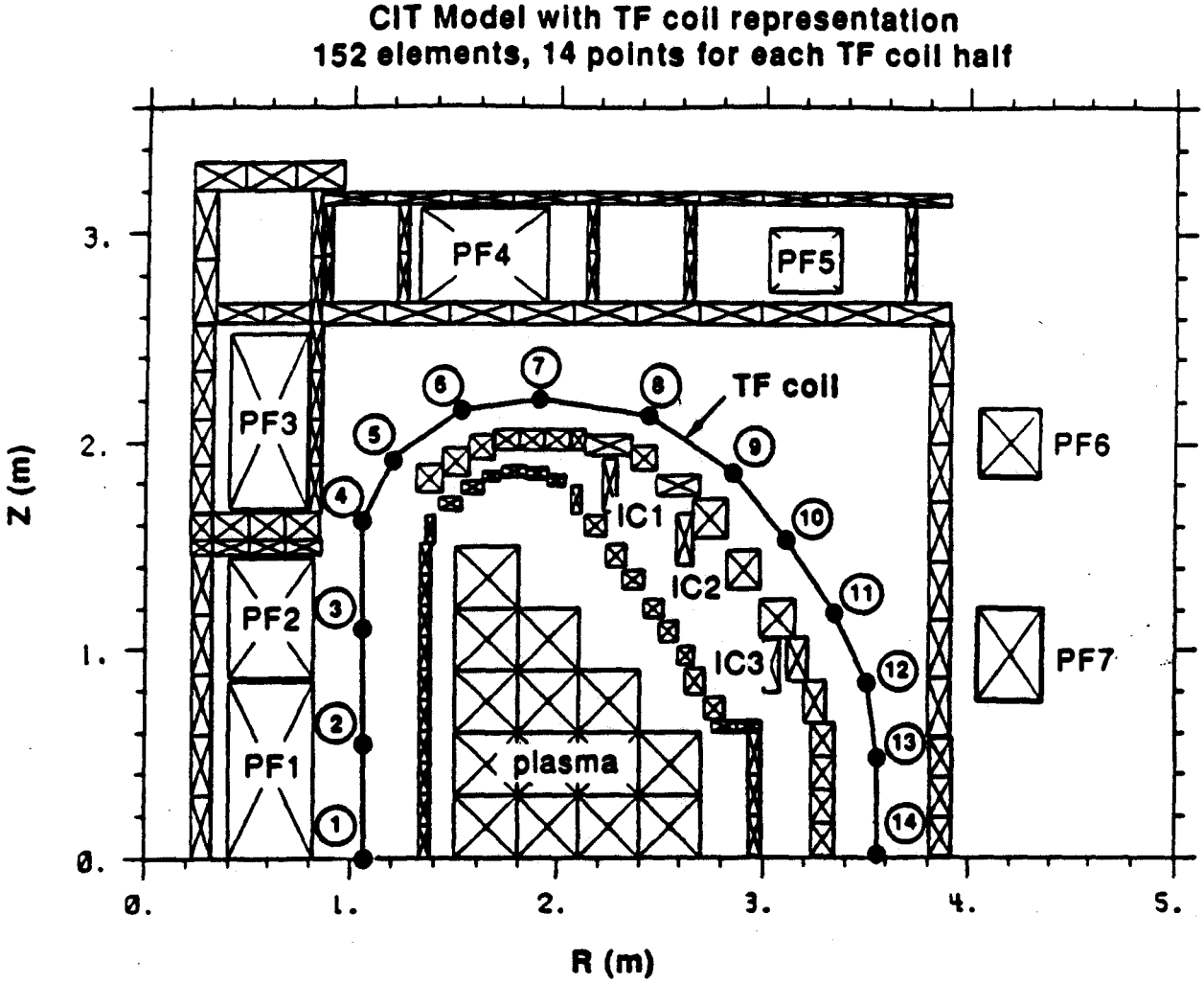

Fig. 2.5.1. CIT Model with TF Coil Representation
PF1 to PF7 are external coils, IC1 to IC3 internal coils

Because the coil temperatures are a major concern, all scenarios investigated have begun beyond the end of the plasma current flattop (EOFT) when most coil temperatures have already reached a value close to their maximum. The currents in the unfaulted coils have been assumed to follow the preprogrammed scenario. Only faults affecting the external PF coils, not the internal IC coils have been considered. From the two groups of faults under consideration, the attention was furthermore constrained to faults whose consequences are likely not to be covered by other faults. Thus the analysis of faults that involve short circuits has been limited to shorts between coil terminals (or leads) which is considered adequate to cover the consequences of shorts to ground or between turns. Shorts of complete mirror coil pairs as well as single coil shorts have been investigated. For cases where coils are driven with undesired voltages, only the application of constant voltages has been analyzed. Table 2.2 lists the scenarios investigated.

An example of how the final scenario selection process was performed is given below. In general, all short circuit scenarios are started at the EOFT because coil currents are high at that time and the plasma still carries its maximum current so that a disruption will be most severe. In case 3, a short in PF1 was chosen because of its high current and its maxima for axial and radial stresses at EOFT. PF1 is a solenoid coil with a large inductance that is located very close to PF2 and PF3. The question was whether the driving currents in the neighboring coils would allow PF1 to reduce its current fast enough so as to avoid temperature problems or whether the high inductance would lead to a slow current decay. A slow decay would also yield a slow reduction of the forces on PF1 and cause larger forces on PF2 and PF3. It would also lead to a change in the magnetic field at the inner leg of the TF coils and cause higher out-of-plane forces. in case 4, similar to case 3, a short was simulated in PF2 to investigate the effect of PF1 on PF2 when PF2 is completely passive and mainly driven by PF1 and PF3. In this case, temperatures are of no concern, but the forces on the solenoid coils and at the inner leg of the TF coils are assumed to be larger. Asymmetric shorts have been investigated for the lower PF2 coil, since those shorts are most likely to occur in the solenoid coils because of the tight lead placement inside the central support structure and the coaxial lead design to reduce the field error. These scenarios have been combined with horizontal and vertical disruptions because then the plasma moves inward and downward towards the solenoid coils.

Table 2.2. List of Fault Scenarios Investigated

type of fault	case	time of fault	description
no fault	0	EOFT	all PF coils driven, plasma rampdown
mirror coil pair shorted stationary disruption	1	EOFT	PF1, PF2, PF3 shorted
	2	EOFT	PF4, PF5, PF6, PF7 shorted
	3	EOFT	PF1 shorted
	3a	EOFT	PF1 shorted, fault detected
	4	EOFT	PF2 shorted
	5	EOFT	PF4 shorted
	6	EOFT	PF7 shorted
mirror coil pair shorted horizontal disruption	7	EOFT	PF2 shorted
single coil shorted horizontal disruption	8	EOFT	PF2 (lower coil) shorted
single coil shorted vertical disruption	9	EOFT	PF2 (lower coil) shorted
constant voltage	10	EOFT	PF1, -1.6kV (voltage at EOFT)
	11	EOFT	PF1, -4kV (full voltage)
	12	EOFT	PF3, 3kV (full voltage)
	13	EOFT	PF4, -6kV (full voltage)
	14	EOFT	PF7, -1.2kV (voltage at EOFT)
	15	EOFT	PF7, -4kV (full voltage)
constant voltage	16	EOPC	PF1, 1.9kV (voltage at EOPC)
	17	EOPC	PF7, 1.3kV (voltage at EOPC)

EOFT: end of plasma current flattop, at t=18.76s for CIT

EOPC: end of plasma current, at t=26.26s for CIT

2.6 MODEL AND SIMULATION METHOD

A two-dimensional model of CIT was used for simulating the fault scenarios. Two versions of this model were used. The basic version is symmetric with respect to the midplane. The second version, which is shown in Fig. 2.5.1, contains elements below and above the midplane, thereby allowing asymmetric behavior to be modeled . It uses a multielement representation of the plasma, leading to a total of 304 elements for the whole cross section. In both versions the TF coil was approximated by a set of straight-line connections between 14 points for each half of the TF coil.

The current scenario in each of the elements was obtained by solving the matrix differential circuit equations. For all fault scenarios, the current in the TF coil was assumed to be constant at a value corresponding to the maximum magnetic field of 11 T at the magnetic axis. The current scenarios were used to obtain the forces on the PF coils and

the out-of-plane forces at each point of the TF coil. Furthermore, the total separating force, overturning moment and torque were computed for each half coil. For all cases the unfaulted PF coils were driven with their preprogrammed currents, assuming that the currents rather than the voltages will be controlled. The initial currents were zero at EOFT in all passive elements and in the IC coils for all scenarios because it was assumed that eddy currents had decayed during the plasma current flattop whereas the PF coil currents change relatively slowly. The plasma and the PF coils were started with their design currents at EOFT. The IC coils were modelled as shortcircuited but not connected in series.

2.7 SIMULATION RESULTS

The forces that occur under fault conditions have been compared with those that occur under normal operating conditions (case 0 in Table 2.2). Multiplication factors for forces and moments were obtained by dividing the maximum value for each force during a fault scenario by the corresponding maximum value under normal conditions when started at EOFT. Multiplication factors greater than 2 were assumed to signal a potential for failure, i.e., the design practices were assumed to embody a safety factor of 2 or higher. An envelope of allowable forces and moments was adopted that constrained failure consequences to multiplication factors larger than 2.

The analysis of the temperature results revealed that the temperature is of no concern for the faults involving shorted coils. In cases where coils are voltage driven, the temperatures will exceed the critical value in any case since adiabatic heating is assumed. Here, an upper temperature limit of 330 K was adopted. However, under all fault conditions, it took a minimum of 4 s to reach this temperature. This implies that corrective actions taken within 4 s or less avoid violation of the temperature limit.

Figures 2.7.1 and 2.7.2 show the maximum multiplication factors for all scenarios. Not included in these data are the cases in which coils PF4 or PF7 are driven with the full available voltage. In all voltage-driven cases, only those results have been included in which the highest temperature in any coil was still below the critical temperature. It can be seen from Fig. 2.7.1, that only coil PF7 shows a multiplication factor for vertical forces that lie outside the allowable range. The maximum factor of 4 occurs only when PF7 is driven continuously with its voltage at EOFT (case 14), while in all other cases the factors are below 2.3. These results show that even when coils with large inductances and high currents (such as PF1) are faulted and the fault remains undetected, the decay time constants are short enough to permit fast current reduction. Also, coils PF5 and PF6 were found to be of very little concern due to their small currents and distant location from the plasma, the solenoid and the TF coils.

The out-of-plane forces on the TF coils were also considered to be covered principally by the design margin. Fig. 2.7.2 shows that only points 5 and 6, which are located at the inner corner of the TF coil, have multiplication factors as high as 4.4. For most cases, and in particular for faults originating in coils PF4 or PF7, large multiplication factors are found. The total force and moments on a half coil show multiplication factors of up to 3.2.

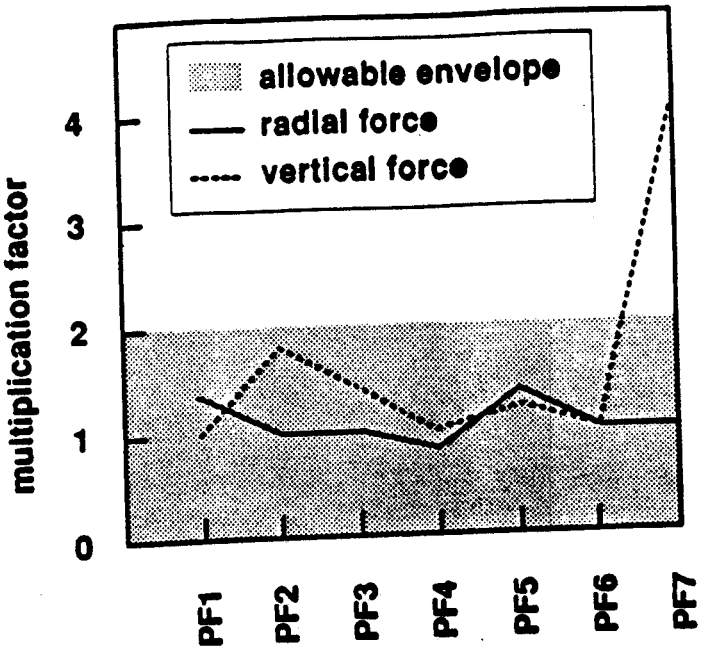

Fig. 2.7.1. Maximum Multiplication Factors for the Forces on the PF Coils Under All Scenarios Except for Cases 13 and 15

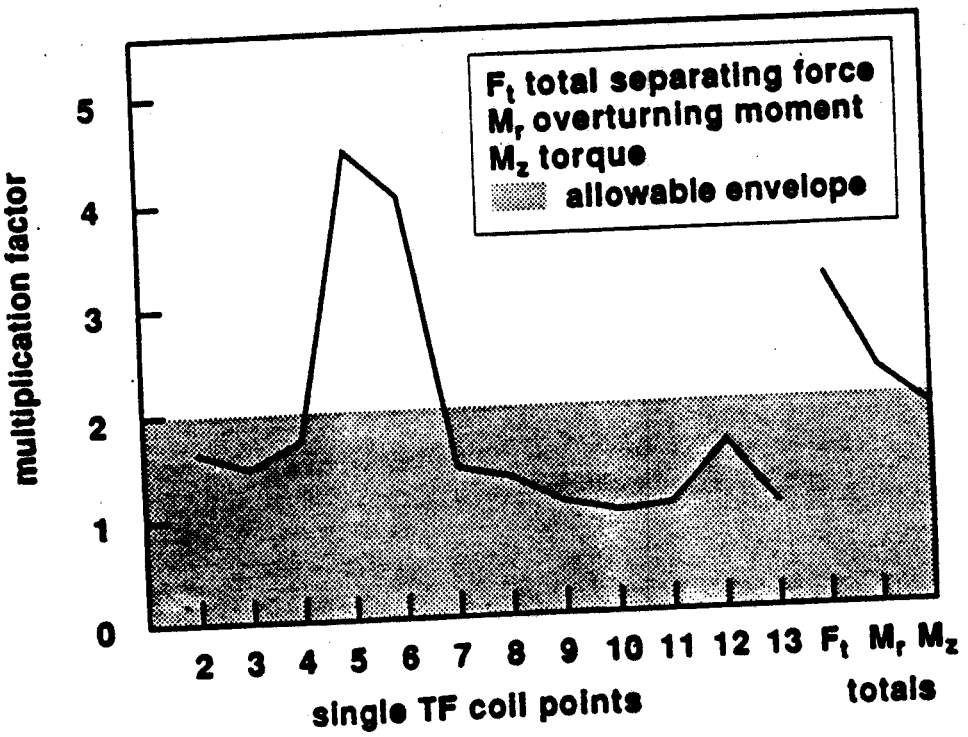

Fig. 2.7.2. Maximum Multiplication Factors for the Out-of-plane Forces on the TF Coils Under All Scenarios Except for Cases 13 and 15

When one of the coil pairs along the outer leg of the TF coil is driven accidentally with its full available voltage, the loads become very severe. A summary is given in Tables 2.3 and 2.4 of multiplication factors for the two cases where PF4 and PF7 are driven to full voltage (cases 13 and 15).

The fault involving PF7 yields high forces on PF7 itself, with a factor of 13 for the vertical direction (compressive force) when the temperature in coil PF7 reaches its limiting value. The distribution of the out-of-plane force along the TF coil perimeter changes in a way to bring the factors for the totals up to 4.2. These effects are still further emphasized for the case when PF4 is driven with its full voltage. PF4 is the coil with the highest voltage because of its strong contribution to the loop voltage at plasma initiation. For this fault, the bursting forces on PF4 achieve multiplication factors of 13 within the first 2 s. At the same time, the out-of-plane forces at the inner corner of the TF coil have reached factors in the same range. Thus, fast detection and protective actions are required to prevent coil damage.

As an example of the effect of mitigating actions, a rapid current rampdown in all coils within 1 s after a detection time of 2 s was simulated for a short in PF1 (case 3a). This reaction reduces the forces on the PF coils very rapidly, but leads to higher out-of-plane forces at the inner corner of the TF coil. More analysis is needed but this example shows that reaction scenarios must be carefully chosen.

No unexpected force reversals of significant magnitude have been found in any of the cases. Also, the effect of the type of plasma disruption was locally constrained and of minor importance when compared with the maxima occurring under normal conditions. However, it was found that the IC coils play a major role in the distribution and the magnitudes of the out-of-plane forces on the TF coils. The IC coils are located close to the plasma and have a strong impact on the local poloidal field. With the IC coils shorted, maximum eddy currents of up to 1.2 MA in the IC coils were obtained. The IC coils will be used to control plasma parameters and cannot be considered as being completely passive. Simulations with controlled IC coil currents (at zero) indicate that, when compared to a circuit with shorted IC coils, the out-of-plane forces were higher by factors of 2 to 4, in particular at the inner corner and less emphasized along the outer leg of the TF coils. Thus, the design of the IC coils and their controls is important for controlling the out-of-plane loads. Simulations using shorted IC coils seem to yield conservative results and it is clear that further consideration is necessary as the coil design solidifies.

coil	radial direction		vertical direction	
	case 13	case 15	case 13	case 15
PF1	1	1.1	1	1
PF2	0.2	0.5	1.2	1.2
PF3	0.9	1.6	5	0.6
PF4	79 (13)*	1.2	19 (2.8)*	0.5
PF5	1	1.4	1	1.5
PF6	1	1	1	1
PF7	1	2.8	1	13

limit temperature reached after 6s

* after 2s

Table 2.3. Multiplication Factors for the Forces on the PF Coils for Cases 13 and 15, Where the Full Available Voltage is Applied Continuously

TF coil point/total	case 13	case 15
2	1.5	1.5
3	1.5	1.4
4	4	1.4
5	38 (14)*	1.5
6	35 (13)*	3
7	1	1.6
8	1	1.8
9	1	1.6
10	1.1	1.8
11	1.1	2
12	1.7	3
13	1	1
F_t	5	4.2
M_r	3.6	3
M_z	1.1	2.8

* after 2s

F_t total separating force on half coil

M_r overturning moment on half coil

M_z torque on half coil

Table 2.4. Multiplication Factors for the Out-of-plane Forces on the TF Coils for Cases 13 and 15, Where the Full Available Voltage is Applied Continuously

2.8 EVALUATION OF FAULT CONSEQUENCES

The potential for high consequence or critical faults seems to be small for the scenarios considered. A reliable and modestly fast detection and protection system should be able to avoid damage to coils or leads and constrain damage to the faulty component. However, if the protection system fails, faults with voltage-driven coils may cause severe consequences. For CIT, the temperature in the driven coil achieved the limiting value of 330 K for every case analysed. At some higher temperature, severe degradation of the insulation involves the potential for turn-to-turn shorts and arcing. Overloads or load redestributions remain the major concern. For normal conducting magnets, overloaded copper will crack which reduces the effective current-carrying cross section of the conductor and leads to additional heating on further operation. This could ultimately cause the temperature-related problems that have already been described. Also, the out-of-plane forces on the TF coils have their highest multiplication factors at the inner corner, which is not directly supported by an external structure. These effects are even more important for superconducting magnets because of the strain sensitivity of the superconducting material. and the danger for the loss of cryogenic stability. In addition, considerable uncertainty still exists about the combined effect of irradiation and mechanical loads on materials and bonding materials.

2.9 CONCLUSIONS

An analysis of potential failures of the TF coil system has shown that a large number of basic failure modes are related to the pulsed operation of the PF coil system. The analysis of interactions of the PF coils system with other reactor systems revealed the intense coupling of those systems. Also, the PF coil power supply and control system is complex and has a potential for fault initiation. Two groups of fault scenarios that initiate in this system, shorts between coil terminals and voltage-driven scenarios, were further examined. A total of 17 fault scenarios were simulated with a two-dimensional model. It was found that shorts do not pose large risks for the magnet system. For scenarios with voltage-driven coils, the temperature limit is also of little concern and a modestly fast protection system will be sufficient. However, for some voltage-driven faults, mainly when coils PF4 or PF7 were involved, high bursting forces on the PF coils were obtained and much larger out-of-plane forces than under normal operating conditions. It was found that the terminal constraint on the IC coils has a strong impact on the distribution and magnitude of the out-of-plane loads but the type of disruption has modest impact on the force distributions. Future work is needed to establish the severity of these effects, their implications for the design of the PF power supply and control system, the design of the protection system, and on the reliability of the overall magnet system.

REFERENCES

1. R. BÜNDE, "Reliability and Availability Assessment of the Next European Torus," *Fusion Technology*, **14**, 197 (1988).

2. L.C. CADWALLADER and D.F. HOLLAND, "Incorporating Reliability into the Design of Experimental Fusion Facilities," *Proc. of the 12th Symposium on Fusion Engineering*, Monterey, California, October 12-16, 1987, part II, p.1262.

3. R. BÜNDE, "On the Availability of the NET Toroidal Field Coils System," *NET/IN/86-39*, Next European Torus (1986).

4. M. PELOVITZ, "TFTR Poloidal Coil Fault Analysis," *Fusion Technology*, **10**, 1059 (1986).

5. R.J. THOME, J.B. CZIRR, and J.H. SCHULTZ, "Survey of Selected Magnet Failures and Accidents," *Fusion Technology*, **10**, 1216 (1986).

6. M. ZIMMERMANN, "A Methodology for the Reliability and Availability Analysis of Magnet Systems for Fusion Reactors," *S.M. Thesis*, Massachusetts Institute of Technology, to be published in 1989.

7. INTOR GROUP, *International Tokamak Reactor: Phase Two A, Part II*, Rep. Intl. Tokamak Reactor Workshop 1984-85, Int. Atomic Energy Agency, Vienna (1986).

8. R.D. PILLSBURY, JR., "PF System for the CIT 2.1m Machine," *MIT-PFC040888*, Plasma Fusion Center, Massachusetts Institute of Technology (1988).

9. S.J. PIET, "Implications of Probabilistic Risk Assessment for Fusion Decision Making," *Fusion Technology*, **10**, 31 (1986).

10. N.L. GREENOUGH, C.L. NEUMEYER, and D. NAYBERG, "TFTR Energy Conversion System: Reliability in the Real World," *Proc. of the 12th Symposium on Fusion Engineering*, Monterey, California, October 12-16, 1987, part I, p.432.

11. J. MCENERNEY et. al., "TFTR Control System Applications - An Overview," *Proc. of the 12th Symposium on Fusion Engineering*, Monterey, California, October 12-16, 1987, part I, p.632.

12. E. BERTOLINI, P.L. MONDINO, and P. NOLL, "The JET Magnet Power Supplies and Plasma Control Systems," *Fusion Technology*, **11**, 71 (1987).

3.0 Preliminary Analysis of Quench Propagation and Voltage Distribution in Superconducting Coils

Marie Oshima

3.1 INTRODUCTION

Two types of cooling are used for superconducting magnets: bath cooling and internal cooling. In bath cooling, the superconductors are immersed in a pool of liquid helium, while with internal cooling, supercritical helium is circulated through passages in the conductors or through a conduit containing the conductor. The latter design, the internally cooled superconductor(ICS), (which also may be called force-cooled superconductor) is evaluated here for safety in fusion applications[2,3,4].

Heat is generated by several sources in a fusion system including nuclear heat deposition, plasma disruption and AC losses[5,6]. These heat sources raise the conductor temperature and may result in a quench (a transition from the superconducting to the normal state without recovery)[7,8]. If quench occurs, a large amount of energy is released and as the helium is heated and vaporizes it can cause large increases in pressure and temperature in the coil. These significant changes in the helium flow may endanger both the magnet system and the refrigeration system. Therefore it is necessary to take these factors into account in the design of superconducting magnets.

Analyses in this report are based on a code originally developed by V.D. Arp[9]. This is a one-dimensional time-dependent program designed to calculate the stability characteristics of an internally cooled superconductor. Its primary purpose was to determine whether or not a given superconductor and flow configuration would be stable relative to a thermal pulse of particular size and duration. Hence, it was limited to a constant current condition or an exponential decay with a fixed decay constant. Since our purpose was to study the failure mode of a superconductor in a nonrecovery condition, the code has been modified by introducing a finite difference form of a circuit equation to represent the coil discharge [10,11].

Three different cases were analysed in this study by using the modified code: recovery, nonrecovery without the finite difference form of the current equation (i.e., constant current), and nonrecovery using the finite difference form (i.e., current decay with nonconstant coil resistance). Future work will involve extensions to this code to improve efficiency, graphical output and ease of use.

3.2 THEORY AND NUMERICAL MODEL

3.2.1 Thermodynamic Analysis

The model[9] assumes that a helium-cooled superconductor is initially at steady-state for $t < 0$, and that a localized heat input Q_0 is then applied to the superconducting coil as is shown schematically in Fig. 3.2.1. The computer program calculates the subsequent thermal behavior of the superconducting coil including temperature and pressure profiles of the helium system.

In the calculations, the following assumptions are made:

1. The length-to-diameter ratio (L/D) of the helium volume inside the conductor is large. Therefore, one-dimensional flow is considered. The helium properties such as temperature, pressure, and velocity are assumed to be uniform over the flow cross section.
2. The helium is assumed to be compressible.
3. Temperature is assumed to be uniform over the conductor cross section.

3.2.1.1 Governing Equations

The governing equations are derived from mass, momentum, and energy equations in terms of the helium pressure, enthalpy, and velocity. Nomenclature is given in Appendix I. The equations are

$$\{\frac{\partial v}{\partial t} = -v\frac{\partial v}{\partial x} - \frac{1}{\rho^*}\frac{\partial P}{\partial x} - F, \tag{3.2.1}$$

$$\frac{\partial P}{\partial t} = -\rho^* c^2 \frac{\partial v}{\partial x} - v\frac{\partial P}{\partial x} + \rho^* \phi(Q_h + vF) \ , \tag{3.2.2}$$

$$\frac{\partial H}{\partial t} = -v\frac{\partial H}{\partial x} - c^2\frac{\partial v}{\partial x} + (1+\phi)(Q_h + vF) \ . \tag{3.2.3}$$

The energy balance equation for the superconducting coil consists of the initial perturbation, joule heating, heat transfer from the conductor to the helium and the axial thermal conduction. The energy balance is given by

$$\frac{\partial T_w}{\partial t} = \left(\frac{Q_0 + Q_j - Q_h}{A_m} + k\frac{\partial^2 T_w}{\partial x^2} + \frac{\partial k}{\partial T}\frac{\partial T_w}{\partial x}\right)/(\rho' C_p') \ . \tag{3.2.4}$$

The heat removal by helium at the conductor surface, Q_h is given by

$$Q_h = P_h h(T_w - T_h) \quad . \tag{3.2.5}$$

The heat transfer coefficient h has been evaluated by both experimental and theoretical studies.[6,9]

Joule heating Q_j includes current-sharing between the superconductor and the copper when the current I is between the critical temperature T_c and the current-sharing temperature T_{cs}. Thus, Q_j is expressed as

$$Q_j = \frac{I^2 \rho}{A_{cu}} f \quad . \tag{3.2.6}$$

where f is given by:

$$f = 0, \quad x < x1, \quad T_w < t_{cs} \quad , \tag{3.2.7}$$

$$f = \frac{T_w - T_{cs}}{T_c - T_{cs}} \quad , T_{cs} \leq T_w \leq T_C \quad , \tag{3.2.8}$$

$$f = 1.0, \quad T_c < T_w \quad . \tag{3.2.9}$$

As the above equations show, if the conductor temperature T_w is lower than T_{cs}, all the current flows in the superconductor, and no joule heating is observed. If T_w is higher than T_{cs}, current flows in the copper and joule heating is observed.

The initial perturbation $Q_0(x,t)$ varies as a function of time and position. As shown in Fig. 3.1, Q_0 is a continuous function in terms of the distance x ($0 \leq t \leq \Delta t$) and is given by

$$\begin{aligned}
&Q_0(x,t) = 0, \quad x < x1, x > x4 \\
&Q_0(x,t) = E_0(1 + sin(\frac{\pi(x - l1)}{w}))sin^2(\pi\frac{t}{\Delta t_h}), \quad x1 \leq x < x2 \\
&Q_0(x,t) = E_0, \quad x2 \leq x < x3 \\
&Q_0(x,t) = E_0(1 - sin(\frac{\pi(x - l2)}{w}))sin^2(\pi\frac{t}{\Delta t_h}), \quad x3 \leq x \leq x4
\end{aligned} \tag{3.2.10}$$

where

$$E_0 = \frac{P_i \rho' A_{cu}}{\Delta t_h},$$
$$x1 = l1 - 0.5w,$$
$$x2 = l1 + 0.5w,$$
$$x3 = l2 - 0.5w,$$
$$x4 = l2 + 0.5w. \qquad (3.2.11)$$

The variables in Eqs.(3.1)-(3.5) are defined as illustrated in Fig. 3.1 and are given as input data (see Appendix II).

3.2.1.2 Boundary Conditions

It is assumed that the pressure in the reservoirs connected by valves to the superconducting coil is constant at both the inlet and outlet. Thus, the boundary conditions are given by:

$$P = P_0 \pm (valve) \times 0.5\rho^* v^2 \quad . \qquad (3.2.12)$$

In Eq.(3.2.12), the negative sign is used for the inlet boundary condition and the positive sign for the outlet. The variables P_0 and *valve* are determined by using the steady-state value of P, ρ^*, and v of the superconductor near the inlet or outlet.

3.2.2 Failure Mode Analysis

When quench occurs, some of the energy is dissipated into the copper stabilizer of the conductor. Under certain conditions, for example, if the energy is dissipated in a small region of the coil, the copper may melt or the insulation may overheat. Another possibility is that the helium pressure may increase to an unsafe level, if not controlled. Thus, it is necessary to ensure that the energy is dissipated in a controlled manner for coil protection.

A superconducting magnet may be protected by a circuit such as that illustrated schematically in Fig. 3.2. The coil is charged by closing the switch and is discharged rapidly by opening the switch. If the switch is opened when quench starts, the initial current is I_0 at $t = t_0$. The magnetic energy initially stored in the inductance L is partially dissipated in the external dump resistor R_d. The variable $R(t)$ represents the time-varying coil resistance. The resistance $R(t)$ takes zero as an initial value and increases monotonically with time in the nonrecovery situation, because the resistive region incapable of recovery grows in size.

There are two potential problems associated with the presence of $R(t)$ in a superconducting coil. First, an unacceptable local temperature rise may occur. Secondly, arcing may be initiated due to an abnormal voltage distribution in the coil.

The governing equation associated with the circuit after the switch is opened is:

$$L\frac{dI}{dt} = -I\Big[R_d + R(t)\Big] \quad . \tag{3.2.13}$$

In a low-current-density system, R_d is often more dominant than $R(t)$. Hence, Eq. (3.2.13) reduces to the following:

$$I = I_o exp(-t/\tau) \quad . \tag{3.2.14}$$

where $\tau = L/R_d$ is the time constant.

However, in a high-current-density system, $R(t)$ may become comparable to R_d, because the normal zone propagates rapidly, and this rapid propagation leads to a rapid increase in $R(t)$. Hence, Eq. (3.2.12) is solved by using a forward integration in time which is based on the finite difference form:

$$I(t_0 + n\Delta t) = I(t_0 + (n-1)\Delta t)\Big[1 - \frac{\Delta t}{L}(R_d + R(t_0 + (n-1)\Delta t))\Big] \quad , \tag{3.2.14}$$

where n is the number of the time increment steps and t in Eq. (3.2.12) is equal to $t_0 + (n-1)\Delta t$. Initial values for current and resistance are given by $I(t_0) = I_0$ and $R(t_0) = 0$ at $n = 1$. In computing the transient, $R(t)$ is recalculated at each instant of time and incremented before it is used in Eq. (3.2.14).

The total resistance $R(t)$ increases with time. At any instant its value is the sum of resistive volume increments. Since the copper area A_{cu} of the conductor cross section is assumed to be constant along the conductor length, the resistance develops with the time and length increments as illustrated in Fig. 3.3 and is given by

$$R(t) = \int_0^{l_n(t)} dR = \int_0^{l_n(t)} \frac{\rho(T)}{A_{cu}} dx \quad . \tag{3.2.15}$$

In the above calculation of $R(t)$, the resistivity is updated at each time increment. The resistivity is a function of temperature and is determined by the physical properties of the conductor.

The resistive voltage propagating along the wire at any point and at any instant in time t is given by

$$V_R(z,t) = \int_0^{l_n(t)} I\frac{\rho(T)}{A_{cu}}dx \quad . \tag{3.2.16}$$

In these calculations, a length of wire which is still superconducting at time t is not involved in the integration of Eq.(3.2.16).

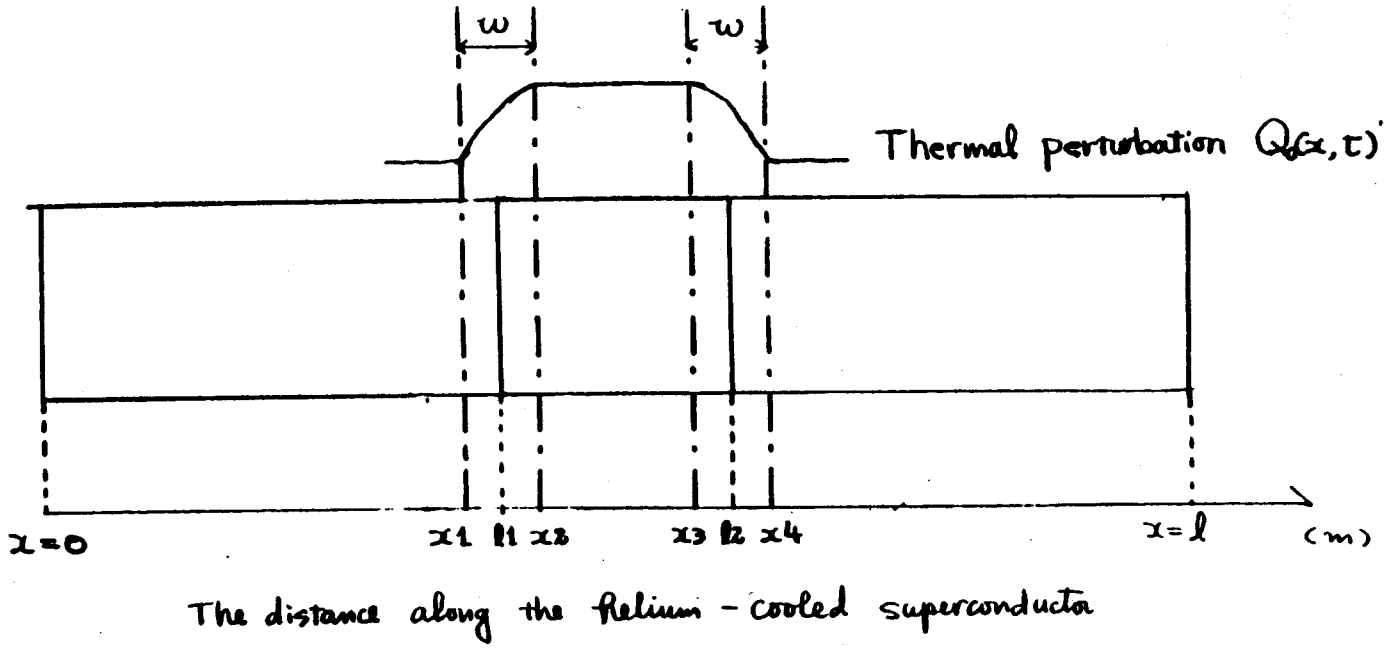

Figure 3.2.1 Schematic Illustration of Helium-cooled Superconductor

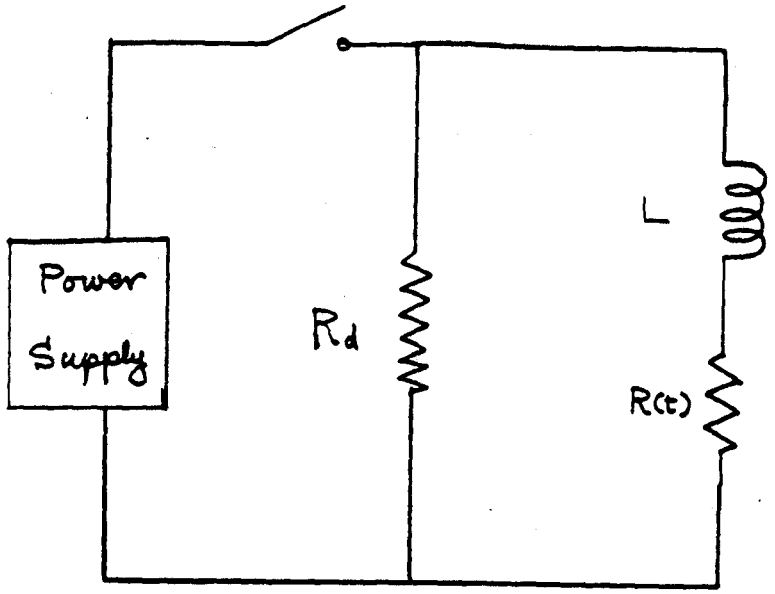

Figure 3.2.2 Schematic Circuit Representing the Superconducting Coil

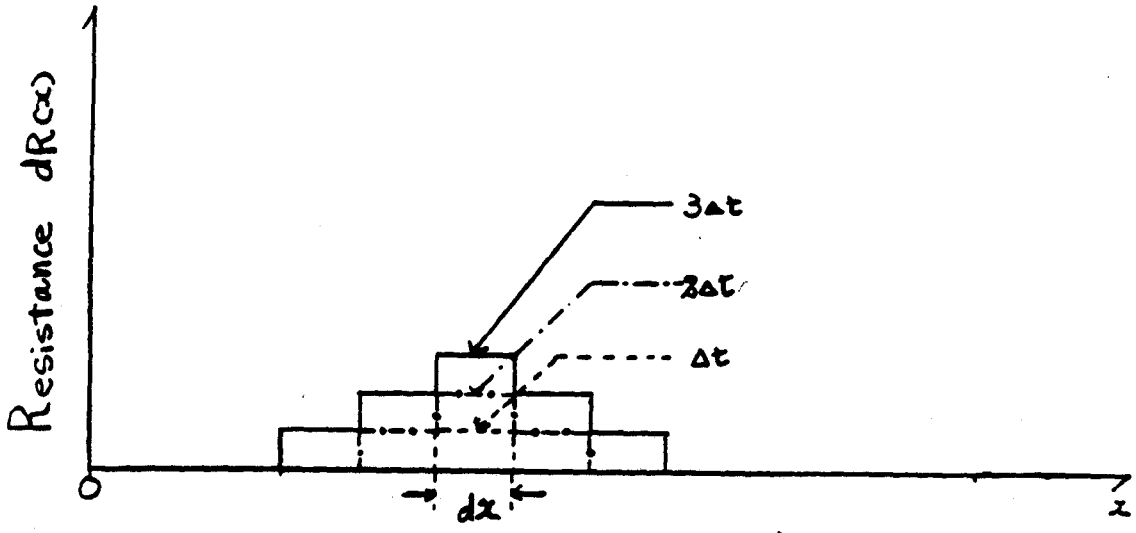

Figure 3.2.3 Schematic Illustration Showing Development of Normal Regions Along the Superconductor at Three Time Increments

3.3 NUMERICAL RESULTS

3.3.1 Computer Program

The computer program originally developed by V.D. Arp[9] was designed to determine both superconductor and forced-flow helium behavior by solving Eqs. (3.2.1)-(3.2.4) presented in Section 3.1[9]. In order to analyze a failure mode, the finite difference form of the circuit equation representing the coil discharge was introduced into the original program for this study. The computer program is run on the Cray computer at MFECC(Magnet Fusion Energy Computer Center).

A simplified flow chart of the computer code is presented and the main structure of the program is summarized in Appendix III. Input data consist of the geometry and physical characteristics of the conductor (components, size and material), operating conditions (magnet field and current), initial helium conditions (temperature and pressure), initial perturbation characteristics (total pulse energy, pulse time and heating length) and time step. Output data consist of the temperature of both conductor and helium, thermal properties of the helium flow, and current and voltage of the conductor after quench at each time step. Then, the output data are stored and can then be used at a later time to generate graphic presentations. Details of the input and output data are given in Appendix II.

The program was modified to stop calculating when recovery is achieved. When non-recovery is observed, the current is recalculated by using the finite difference form of the equation representing the discharge circuit (Fig 3.2) and iteration is continued until temperature or pressure reaches a predetermined limit.

The criteria for recovery are the following:

1. $t > 2\Delta t_h$
2. $T_w < T_{cs}$
3. $T_h > T_{cs}$

If these criteria are violated, the superconducting coil cannot recovery, which is the case of interest for this study.

3.3.2 Sample Numerical Results

The computer program modified for this study analyzes the recovery or quench propagation of a Nb_3Sn superconducting coil. Three test case analyses are presented: recovery

(case 1), and nonrecovery with and without the finite difference form of the discharge circuit equation (cases 2 and 3). Appendix II-(2) shows the operating conditions for each case.

3.3.2.1 Recovery Case

Figs. 3.1 and 3.2 show the current and resistive voltage profiles over a superconducting coil as a function of time. Figs. 3.3 - 3.5 show conductor and helium temperature, and helium pressure profiles in the middle of the coil ($x = 44.0$ m) as a function of time. Since this is the recovery test case, current is constant as seen in Fig. 3.3.1. Resistive voltage and conductor temperature have peak values at $t = 0.075$ s as is shown in Figs. 3.3.2 and 3.3.3. Characteristic recovery behavior can be seen in Figs. 3.3.2. and 3.3.3. The initial heat perturbation causes the conductor temperature to increase until it reaches a peak value. Then it starts to decrease as it is cooled by the helium, and finally the temperature of both the conductor and helium become equal. The resistive voltage in the copper rises as the temperature increases.

Figs. 3.3.6 - 3.3.9 describe conductor and helium temperature, resistive voltage and helium pressure at $t = 0.0025$, 0.005 and 0.06 s as a function of position along the conductor. Since the helium has enough heat capacity to cool the conductor against the initial heat perturbation, the temperature of the conductor increases locally for a short time, but then quickly decreases to the superconducting temperature range (Fig. 3.3.6). The helium temperature changes in relation to the conductor temperature as shown in Fig. 3.3.7. Fig. 3.3.8 also shows that the resistive voltage increase corresponds to the temperature increase, but returns to zero after recovery is achieved.

Heated helium spreads with the velocity of sound beyond the initially heated zone due to adiabatic compression of the helium as is shown in the pressure profile of Fig. 3.3.9.

3.3.2.2 Nonrecovery Case at Constant Current

- Without the Finite Difference Form of the Discharge Equation -

Here, the total initial heat pulse is larger than that used the case presented in Section 3.2.1 in order to obtain nonrecovery. Since the circuit switch is assumed to be closed even after quench, the finite difference form for discharge is not applied to this case. Hence, there is no current decay as seen in Fig. 3.3.10, which is a graph of the current profile as a function of time. Fig. 3.3.11 shows the resistive voltage across the conductor as a function of time. The slight discontinuity at $t = 1.25$ s is caused by the computing time increment algorithm, because the time increment automatically becomes large when nonrecovery starts. Fig. 3.3.12 shows profiles of the conductor and helium temperatures at the middle of the conductor ($x = 44.0$ m). The helium flow initially cools the conductor, but the temperature increases because the helium does not have enough heat capacity relative to

the large initial heat perturbation. As a result, system loses its cooling capacity because of excessive joule heating and the temperature rises.

Figs. 3.3.13 - 3.3.15 show the conductor and helium temperature profiles, and the resistive voltage profile at $t = 0.0025$, 0.0075 and 2.11 s as a function of a position along the conductor. The temperature increase seen in these figures indicates that the normal region is propagating. As the normal region grows, the temperature becomes higher due to the increase in joule heating at constant current. This results in an increase in the resistive voltage. Fig. 3.3.16 shows the helium pressure profile as a function of position. Helium pressures at this high level are beyond the accuracy of the correlations in this code. Future modifications are required to obtain accurate output data at high pressure levels.

3.3.2.3 Nonrecovery Case with Current Decay

- With the Finite Difference Form of the Discharge Equation -

Unlike the condition in Section 3.3.2.2. once nonrecovery occurs the circuit switch (Fig. 3.3.2) is opened. In order to model this effect, the finite difference form of the discharge equation is applied to the calculations.

Figs. 3.3.17 and 3.3.18 show the current and resistive voltage profiles across the conductor as a function of time. The nonrecovery situation is obtained at $t = 0.11$ s, but the discharge circuit causes the current to decay rapidly as shown in Fig. 3.3.17. This current decay results in a decrease in the resistive voltage. Although the resistive voltage is a function of temperature, the decrease in the resistive voltage is caused principally by the current decay. The conductor and helium temperatures become constant after 5 s as shown in Fig. 3.3.19.

Figs. 3.3.20 and 3.3.21 show the temperature profiles of conductor and helium at $t = 0.0025, 4.11$ and 15.11 s as a function of position. The temperature in each increases to 120.0 K. The resistive voltage shows a different behavior from that in case 3.3.2.2 because of the current decay. As is shown in Fig.3.3.22, the entire voltage increases in $t = 4.11$ s and decreases to about zero in correspondance with the current decay, because the current also becomes zero at $t = 15.11$ s. The helium pressure grows to 200 atm as shown in Fig. 3.3.23, but this is below that reached in the previous constant current case.

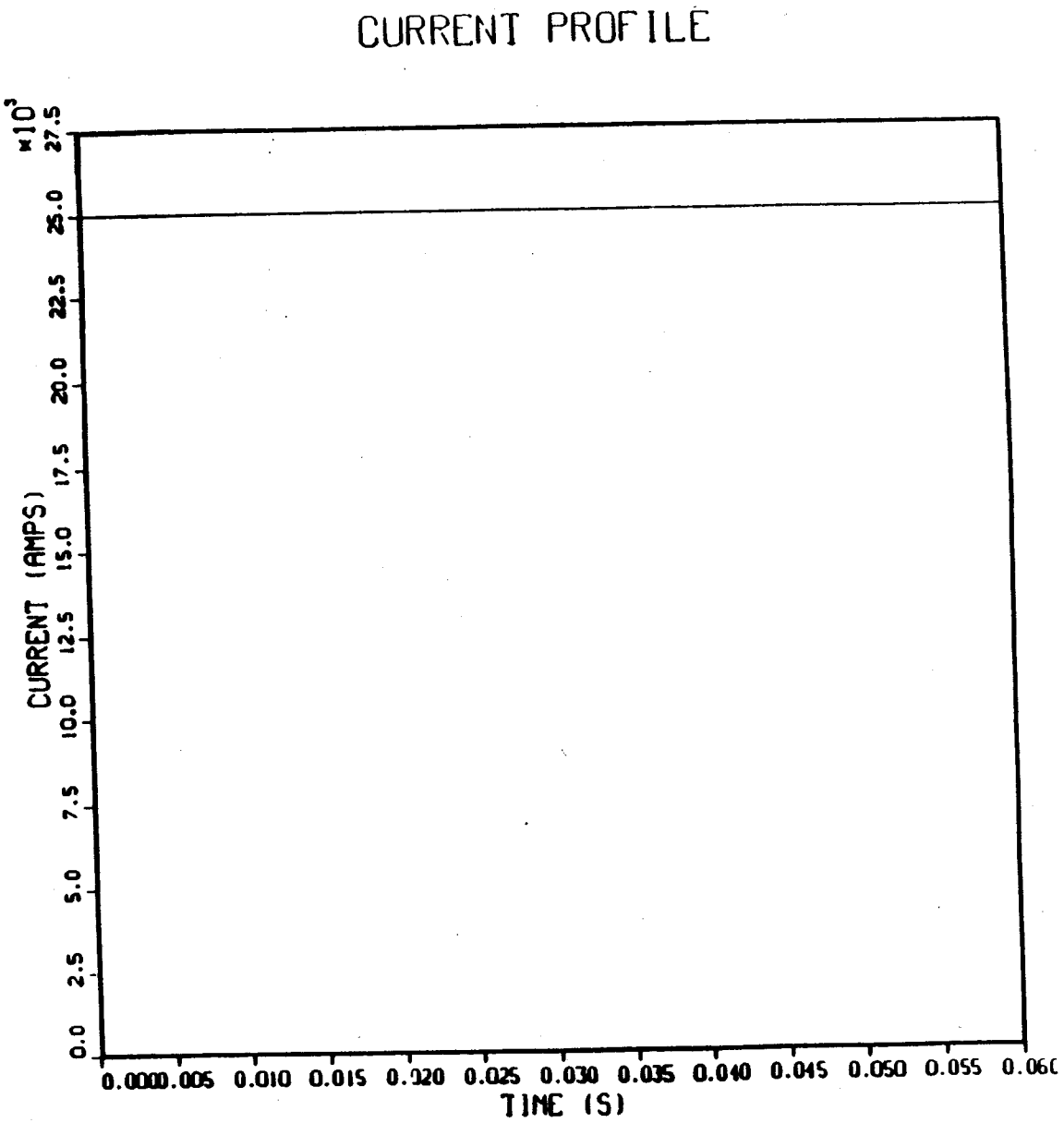

Figure 3.3.1 Current Profile as a Function of Time, Case 1

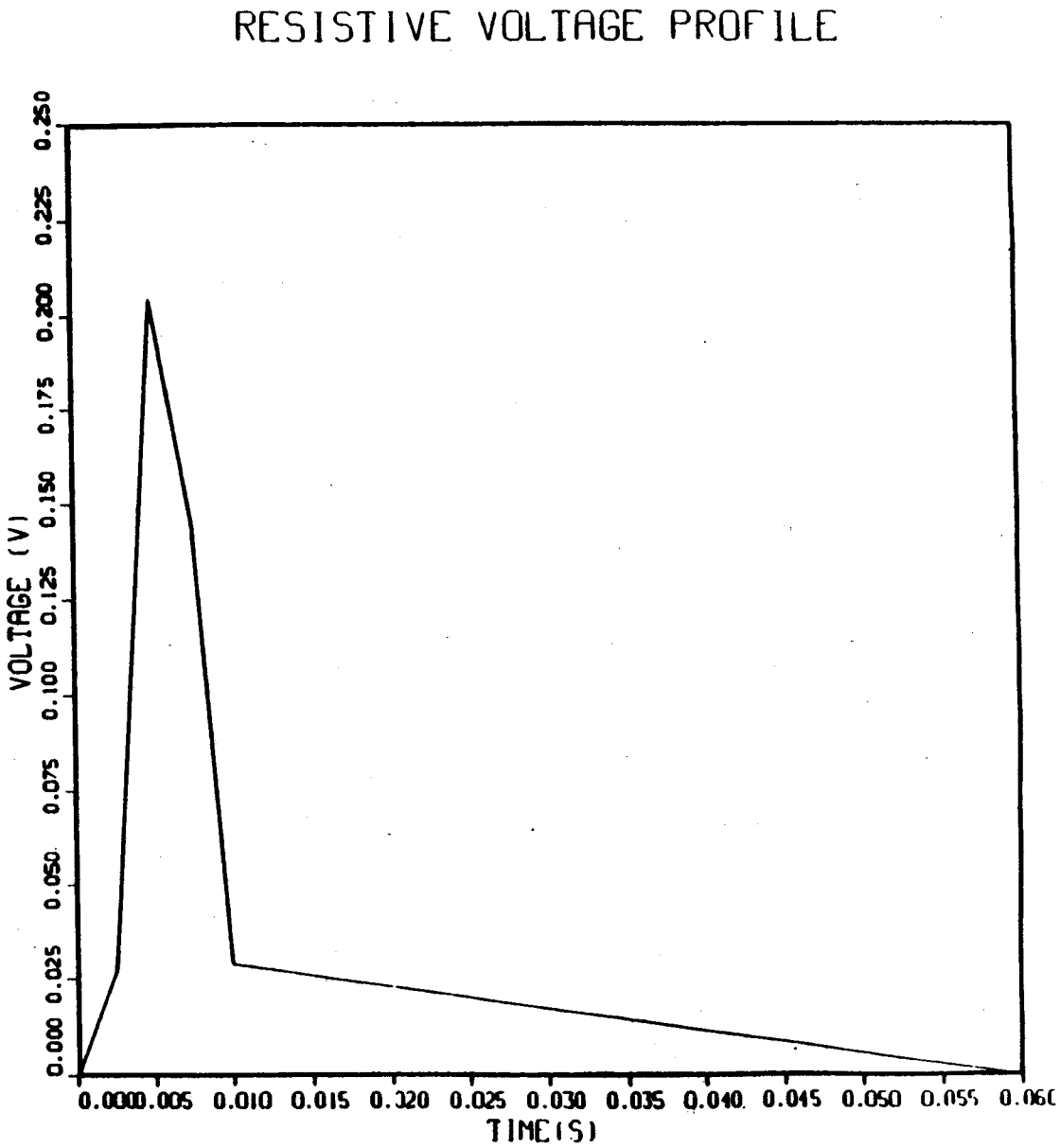

Figure 3.3.2 Resistive Voltage Profile as a Function of Time, Case 1

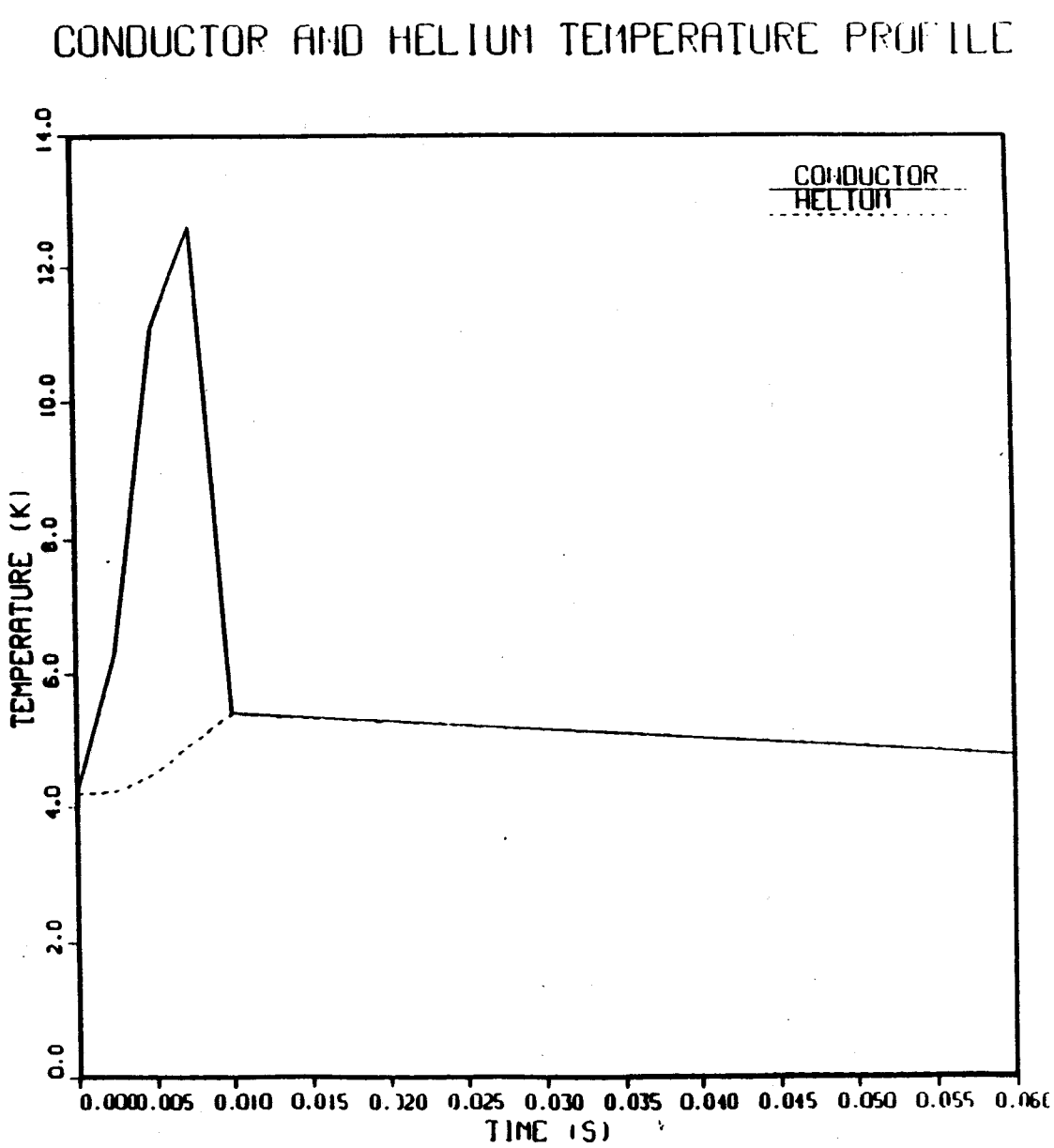

Figure 3.3.3 Conductor and Helium Temperature Profiles at the Center of the Conductor vs Time, Case 1

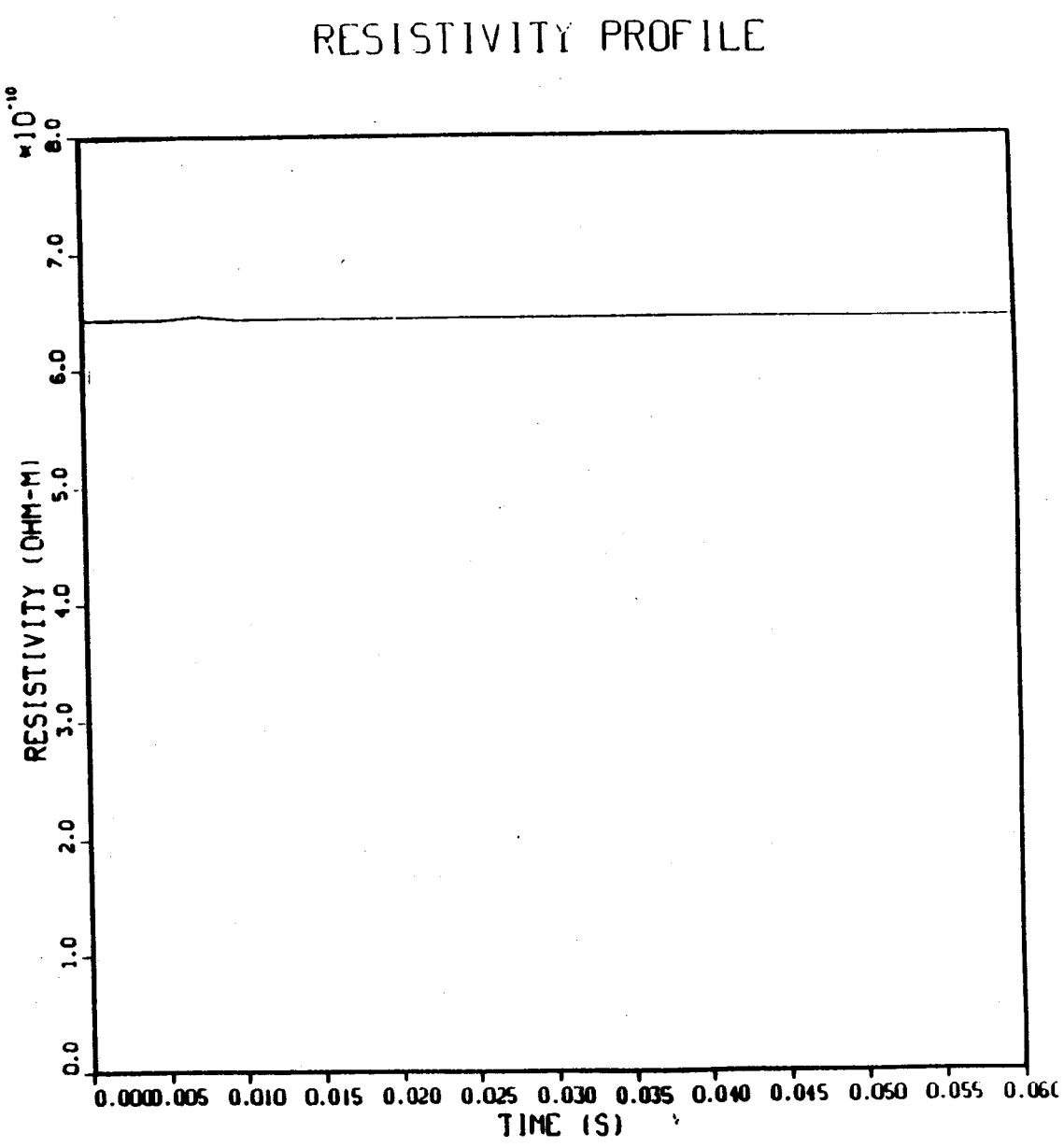

Figure 3.3.4 Resistivity Profile at the Center of the Conductor vs Time, Case 1

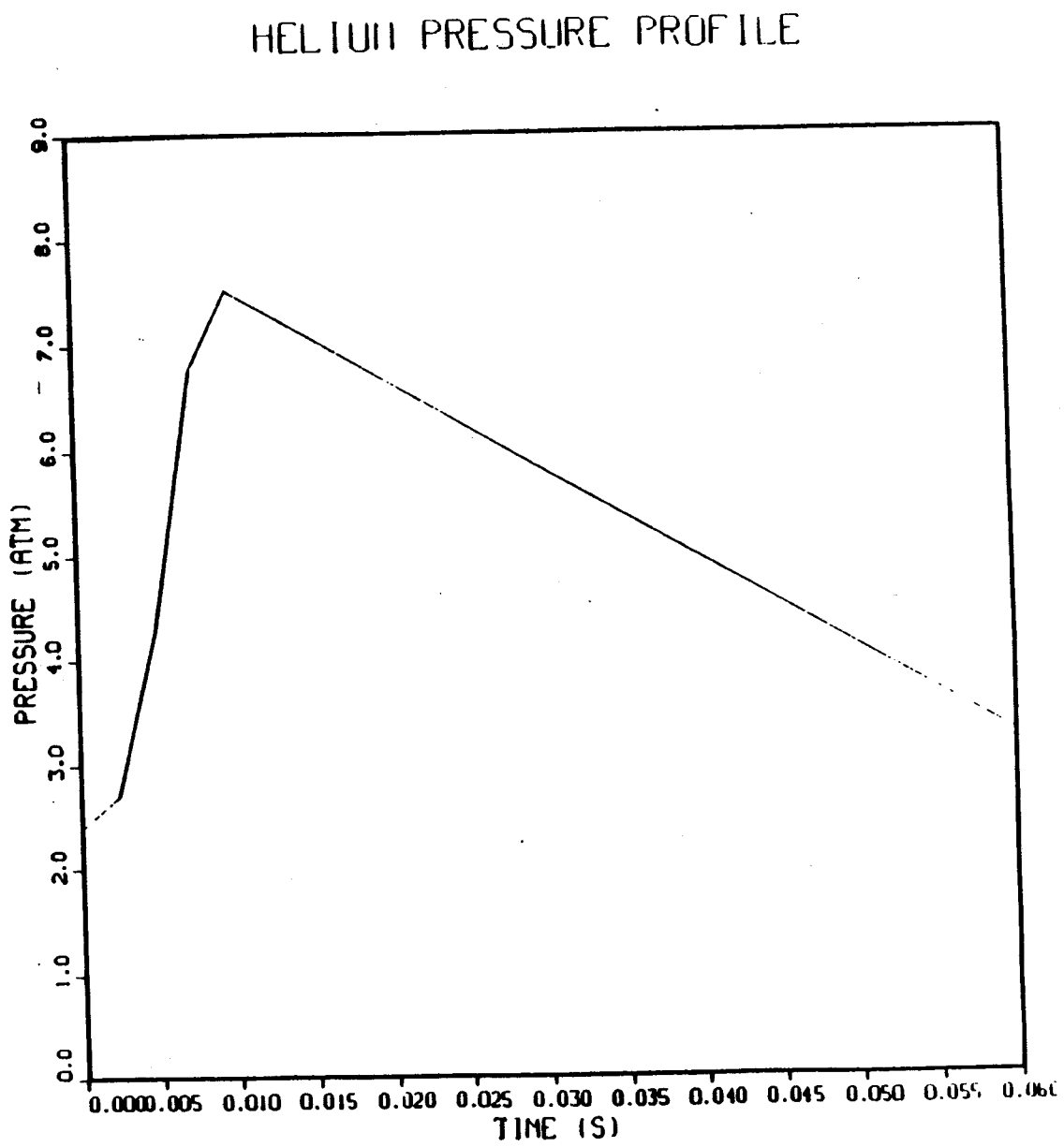

Figure 3.3.5 Helium Pressure Profile at the Center of the Conductor vs Time, Case 1

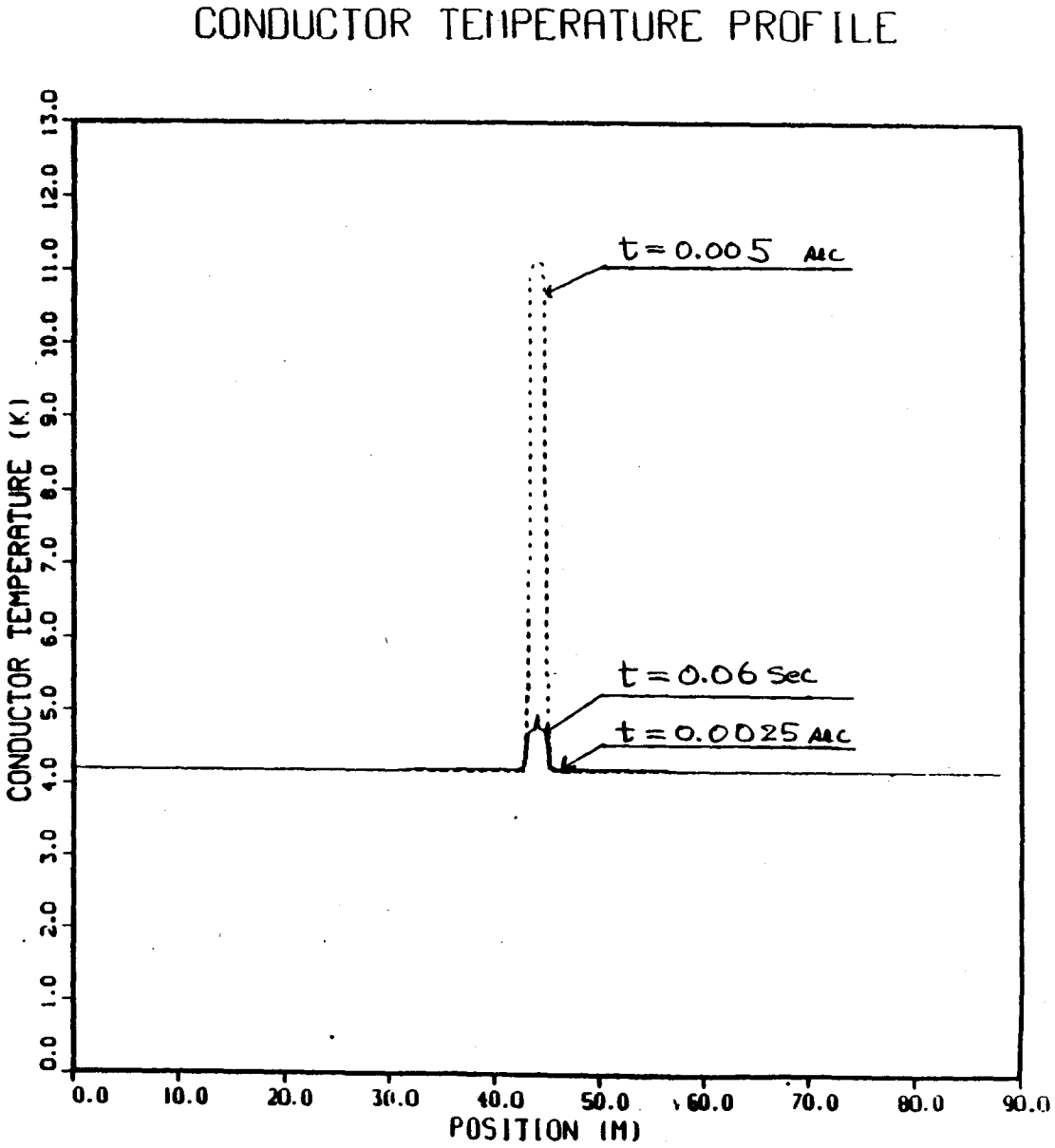

Figure 3.3.6 Conductor Temperature Profile at Three Times vs Position, Case 1

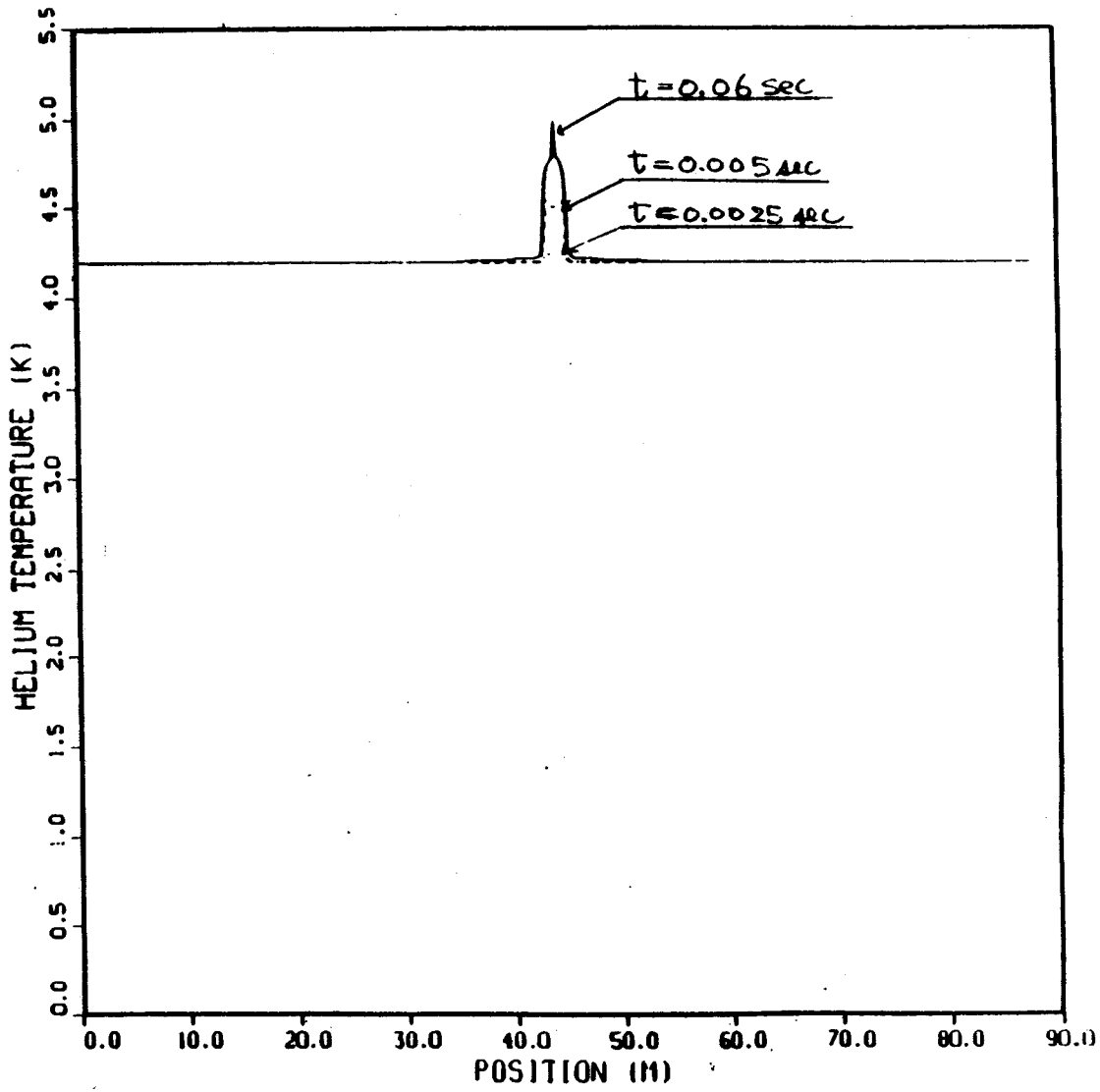

Figure 3.3.7 Helium Temperature Profile at Three Times, Case 1

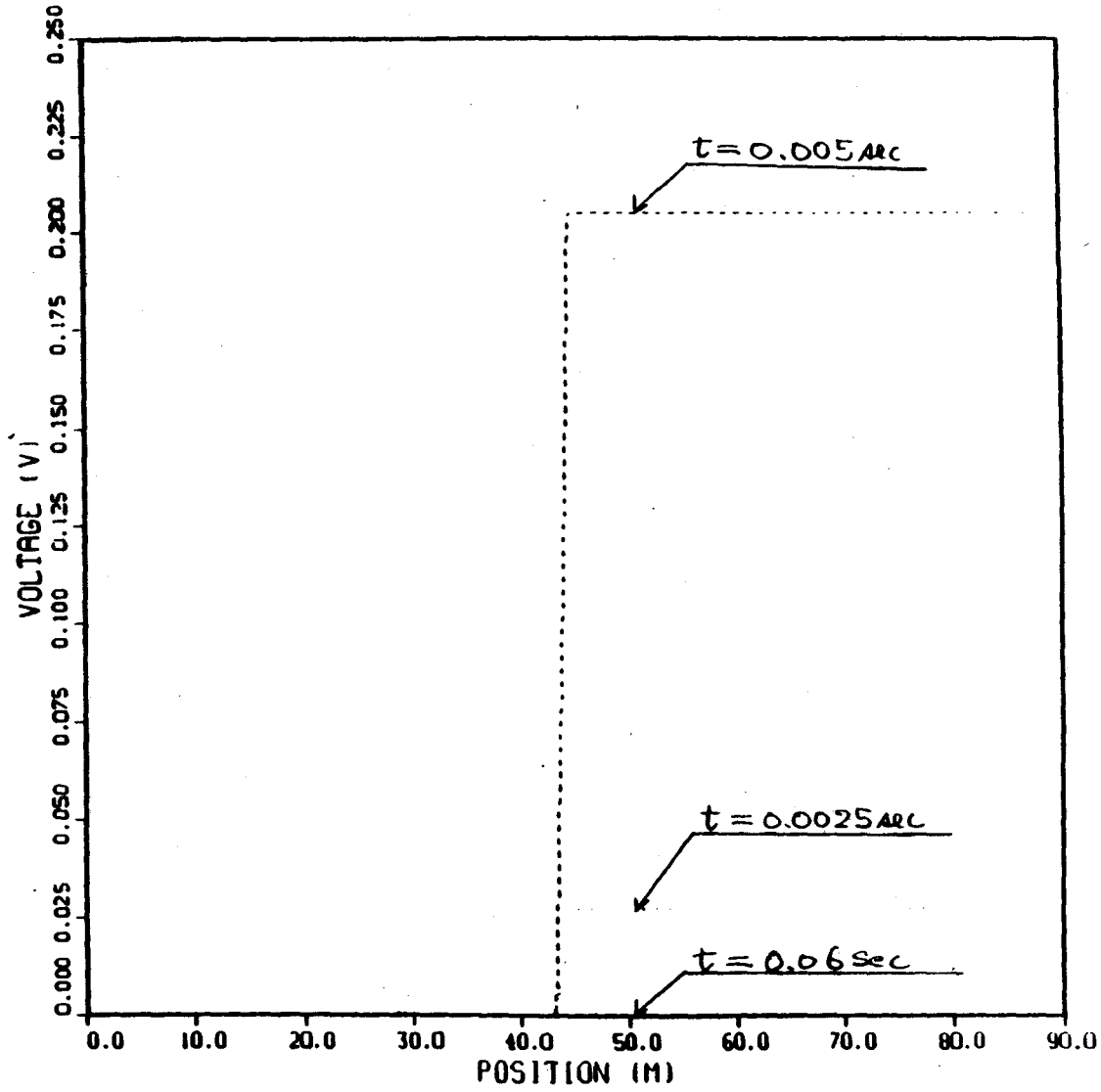

Figure 3.3.8 Resistive Voltage profile at Three Times vs Position, Case 1

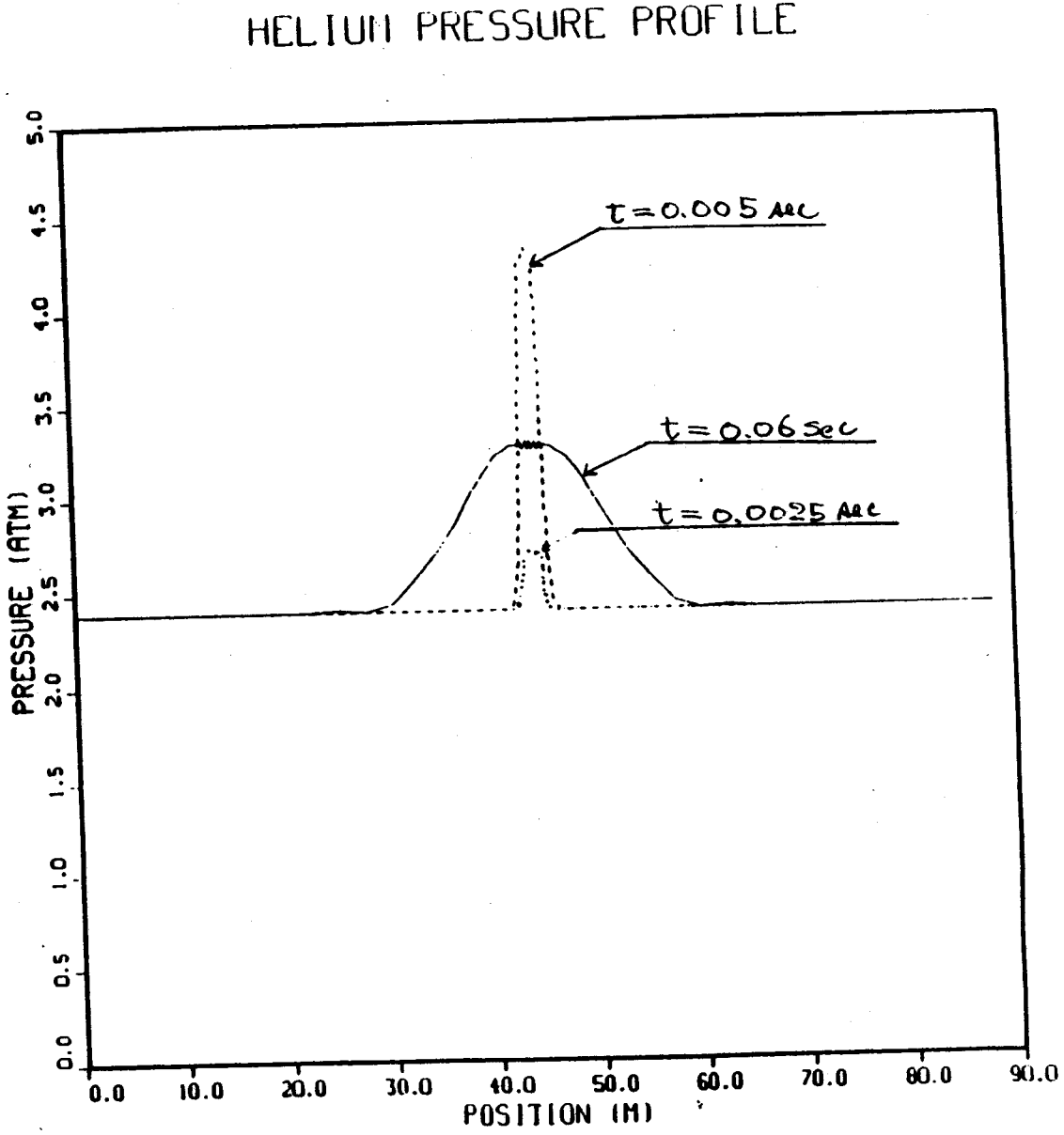

Figure 3.3.9 Helium Pressure Profile at Three Times vs Position, Case 1

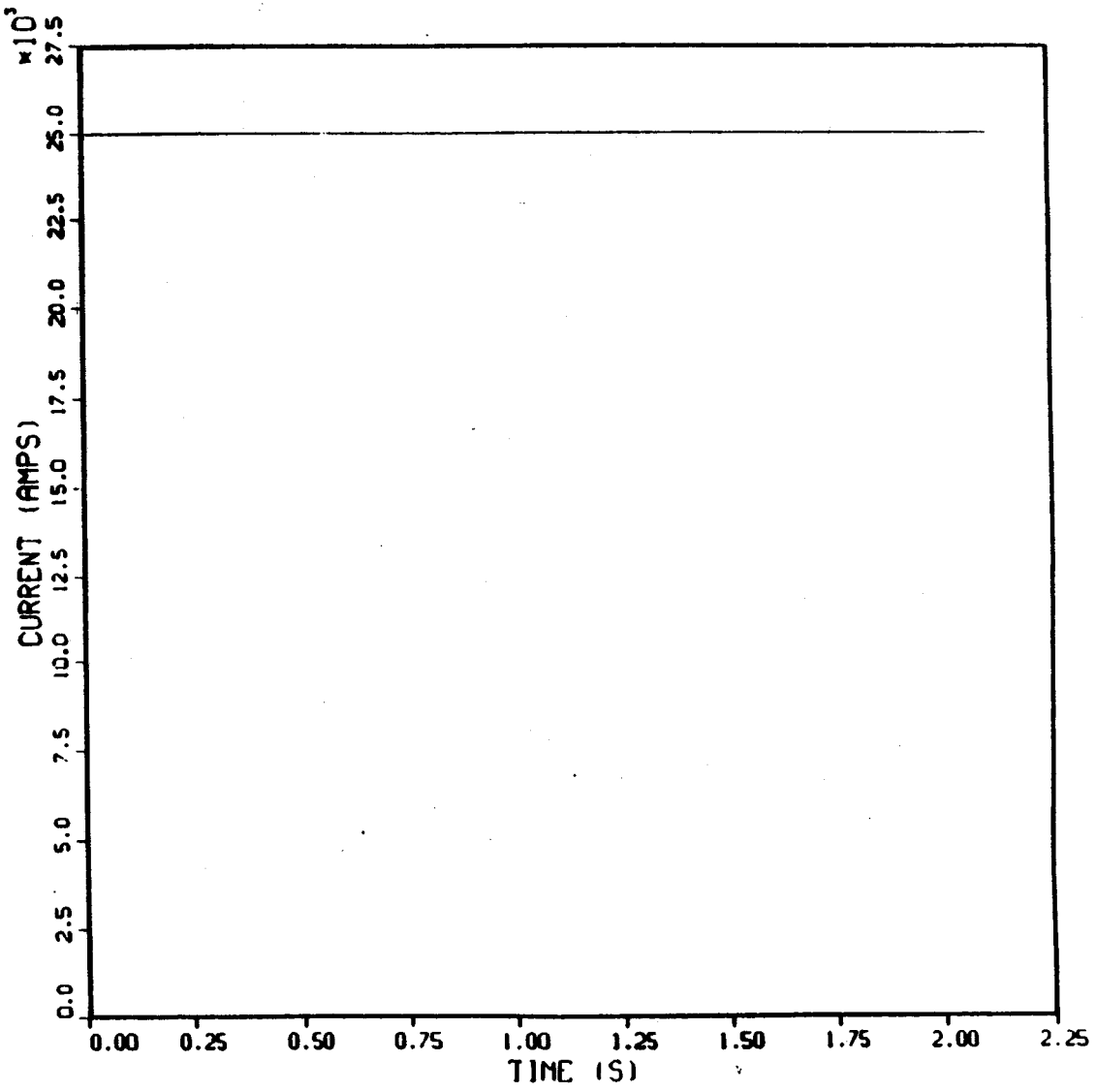

Figure 3.3.10 Current Profile as a Function of Time, Case 2

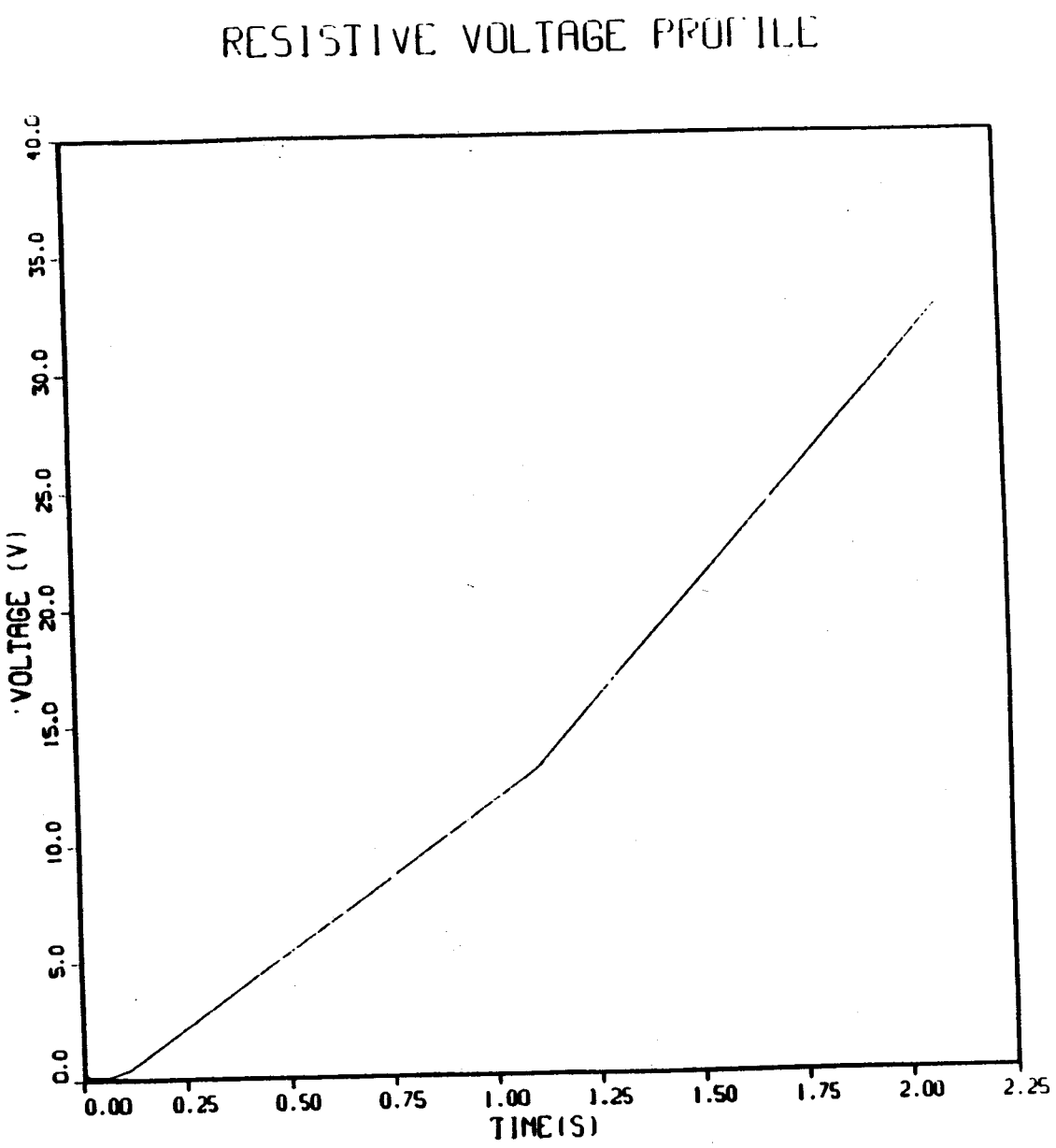

Figure 3.3.11 Resistive Voltage Profile as a Fuction of Time, Case 2

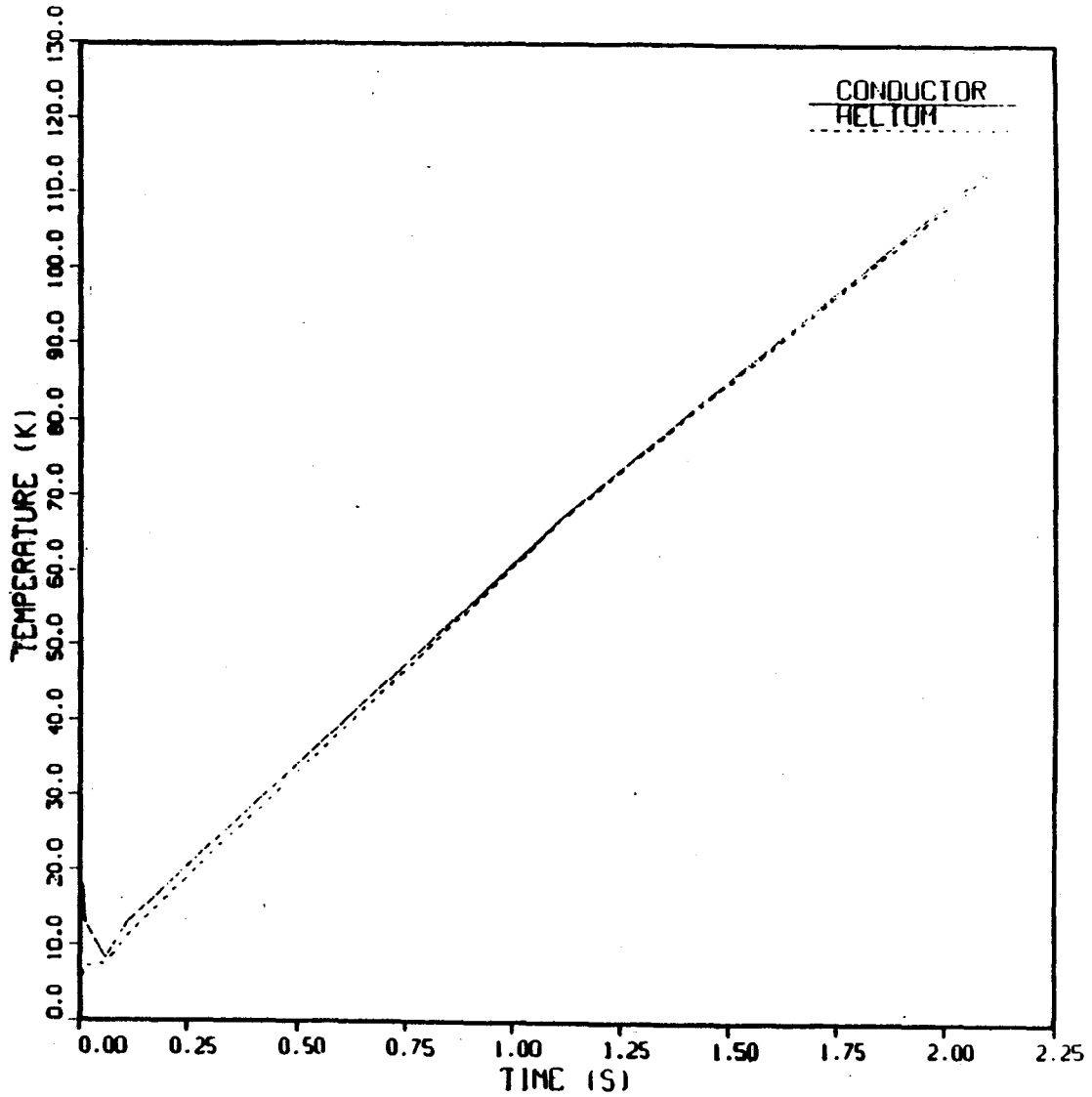

Figure 3.3.12 Conductor and Helium Temperature Profiles at the Center of the Conductor as a Function of Time, Case 2

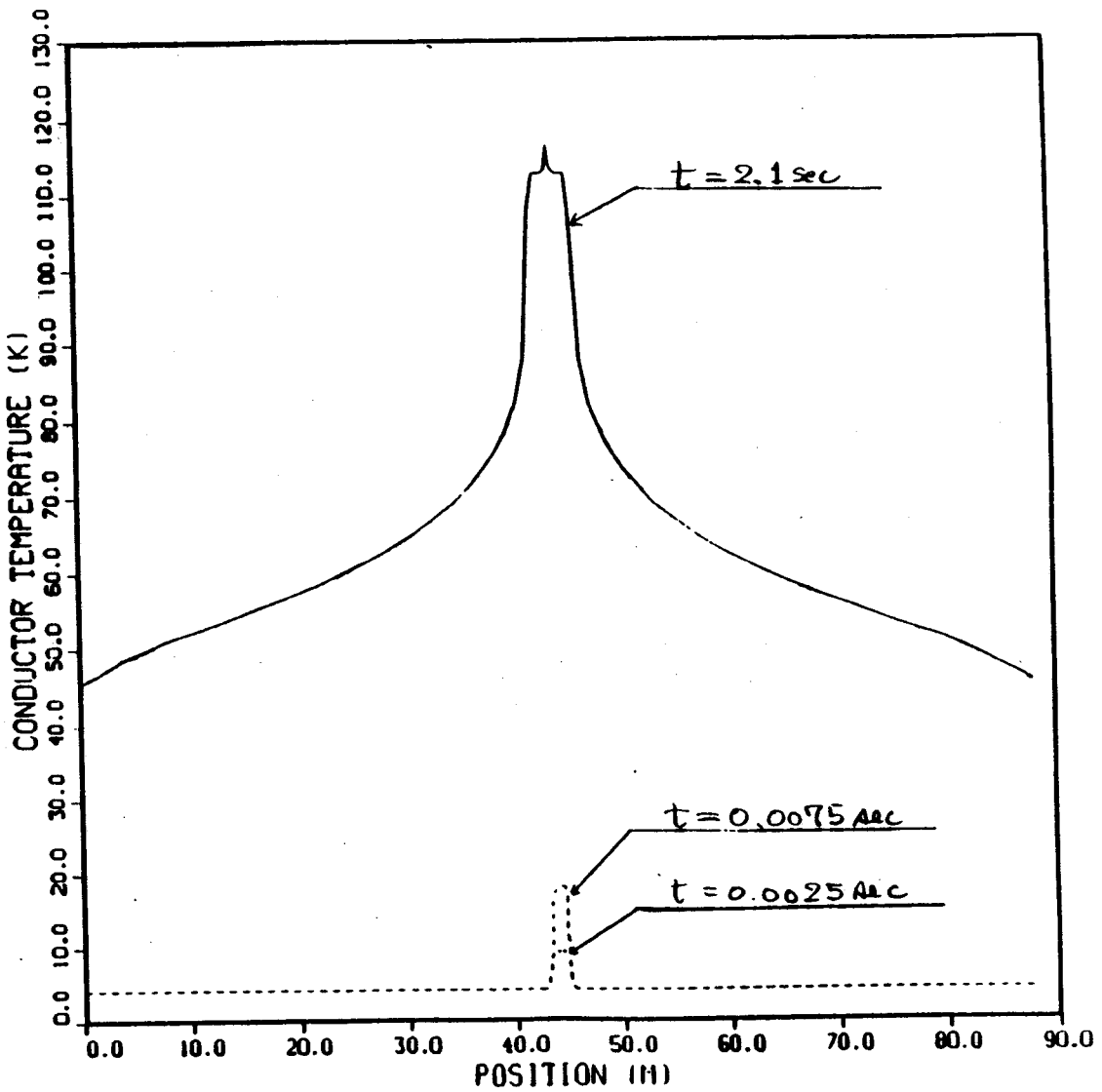

Figure 3.3.13 Conductor Temperature Profile at Three Times vs Position, Case 2

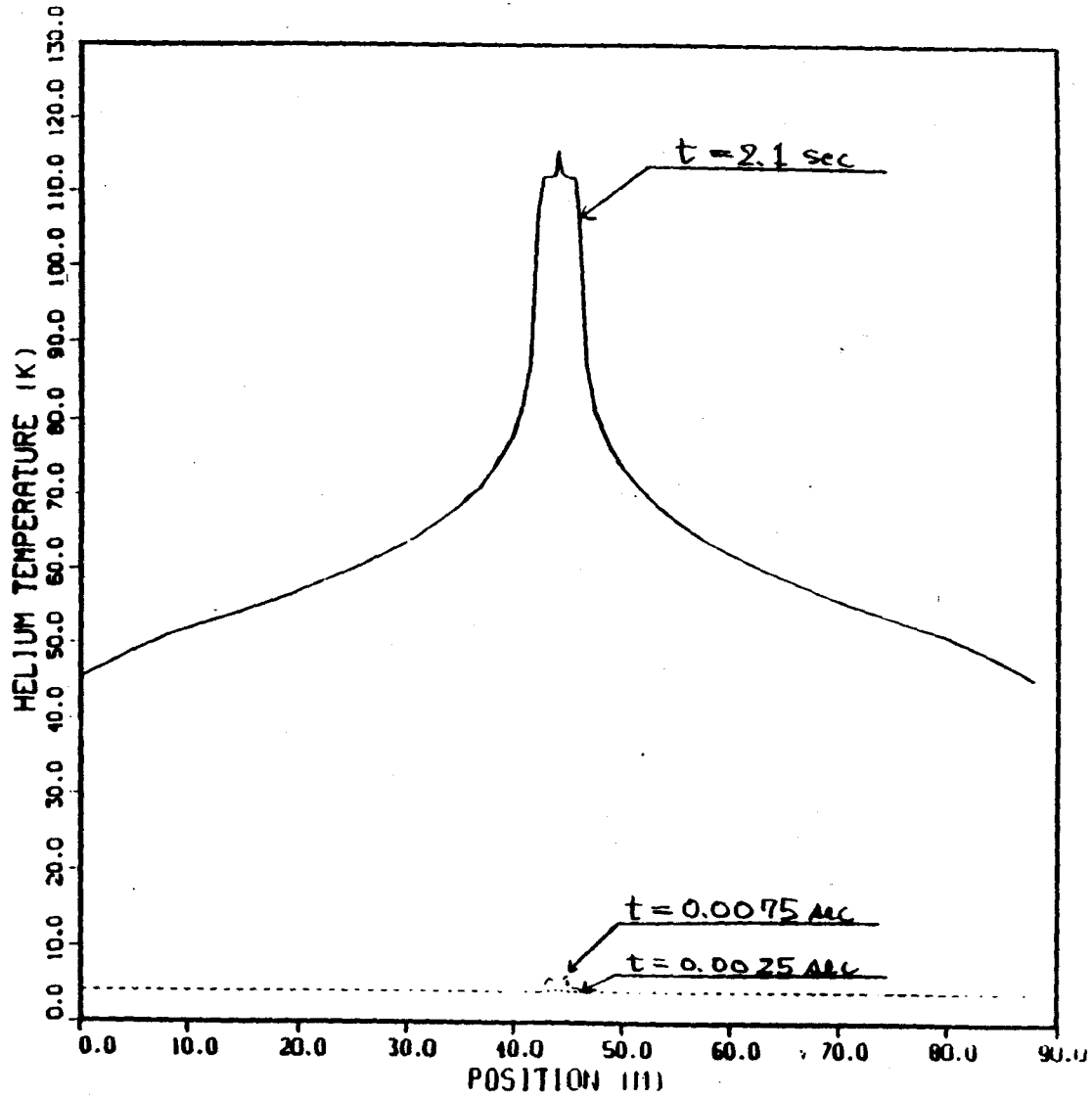

Figure 3.3.14 Helium Temperature Profile at Three Times vs Position, Case 2

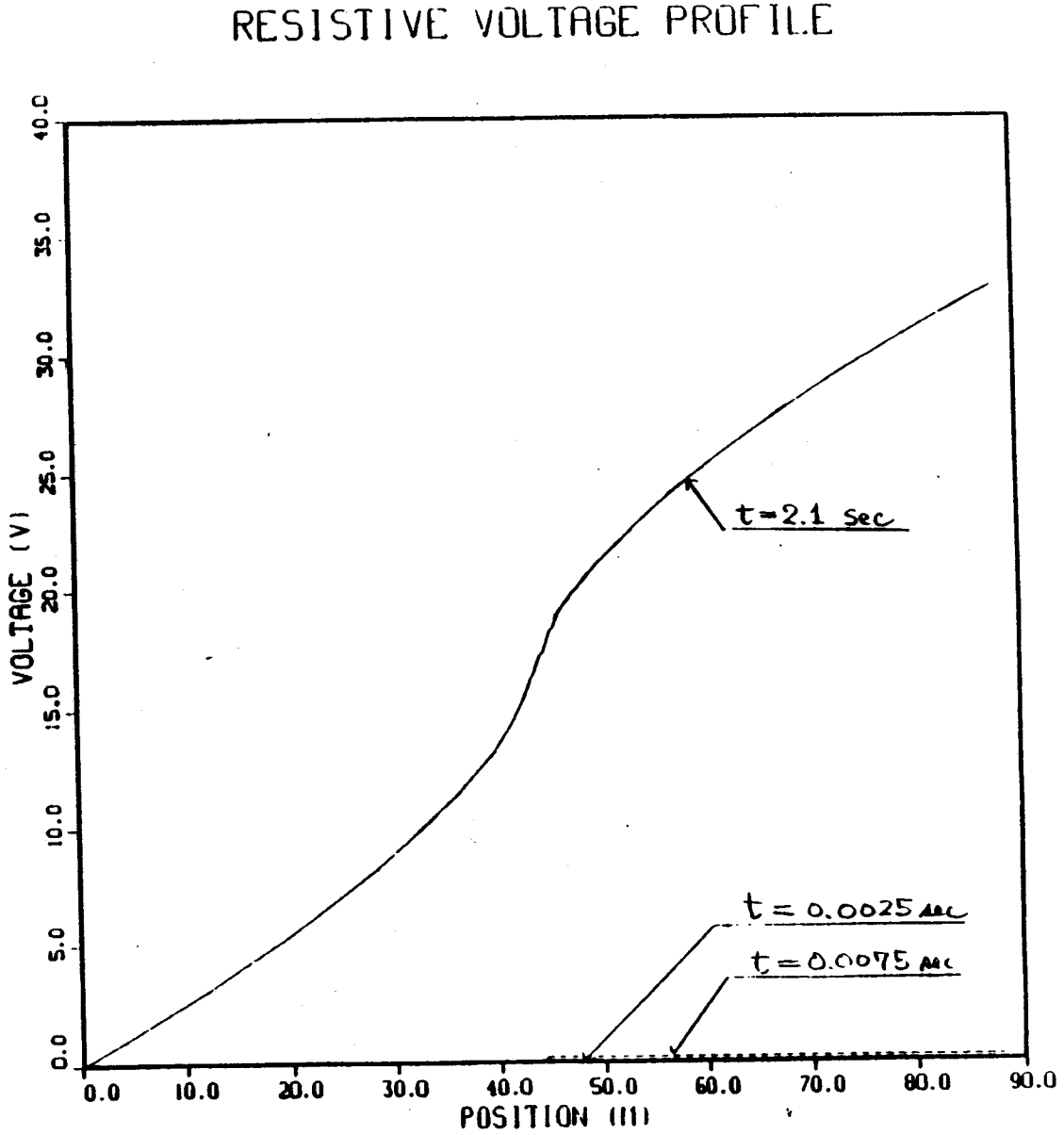

Figure 3.3.15 Resistive Voltage Profile at Three Times vs Position, Case 2

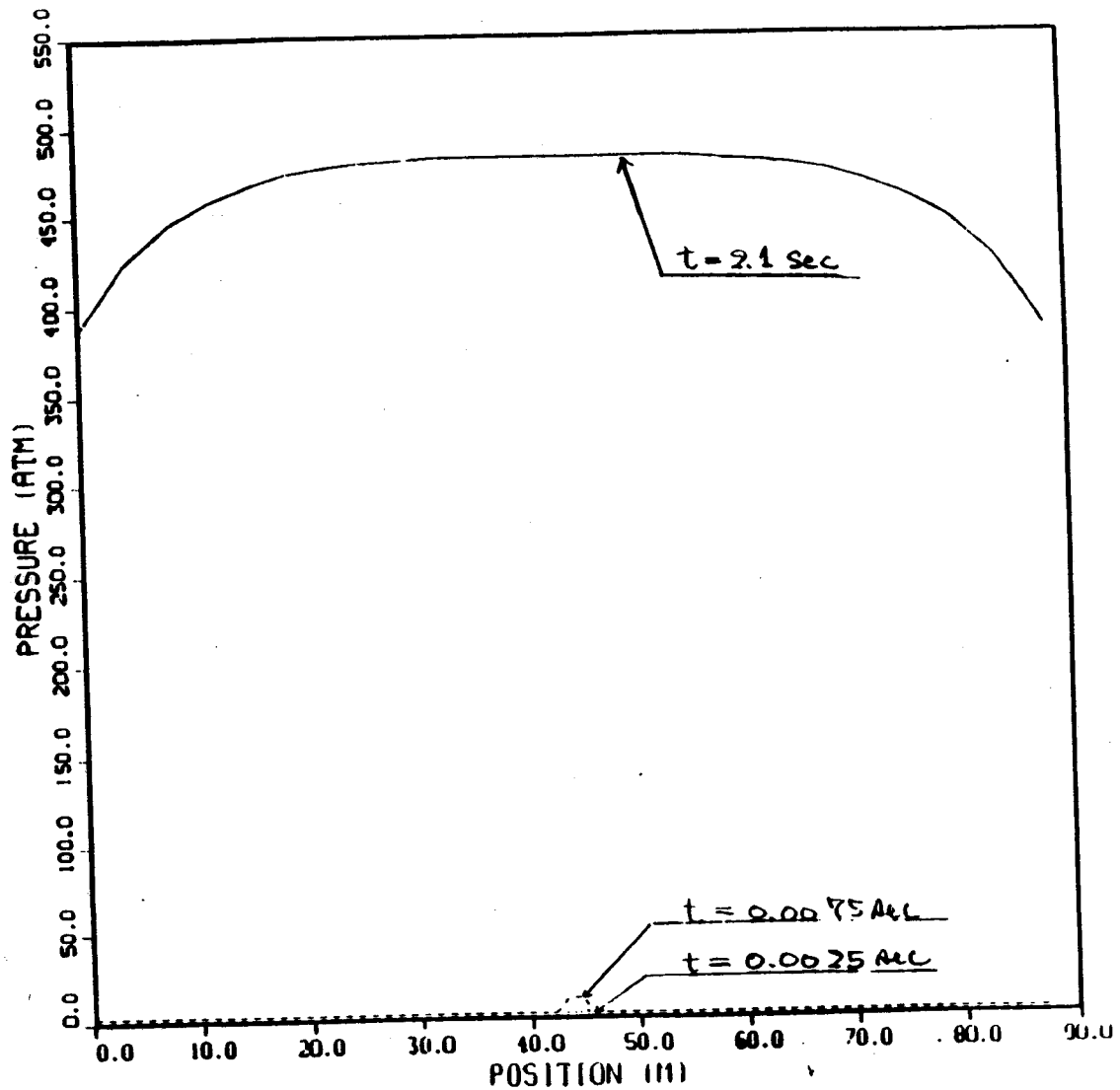

Figure 3.3.16 Helium Pressure Profile at Three Times vs Position, Case 2

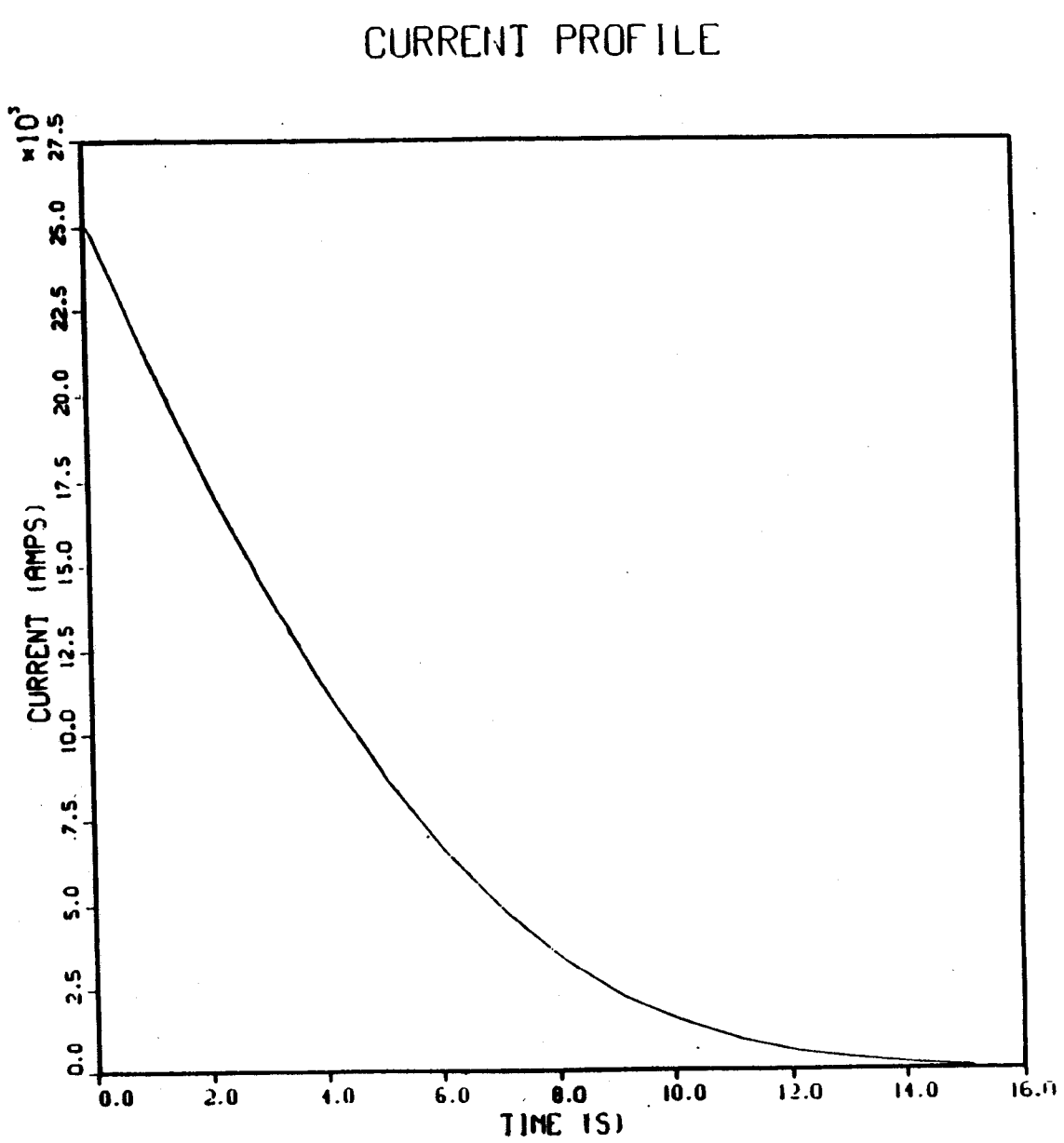

Figure 3.3.17 Current Profile as a Function of Time, Case 3

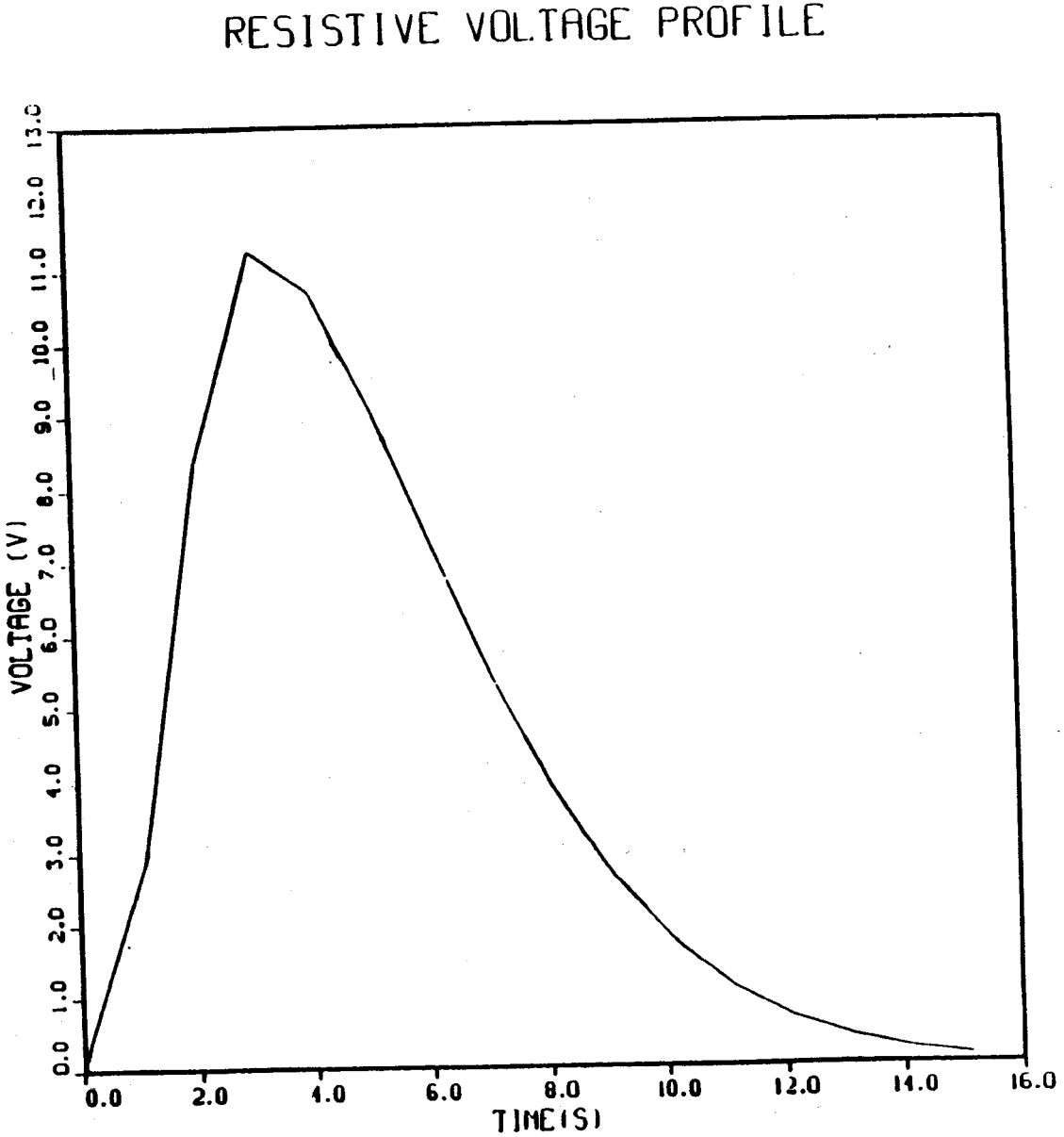

Figure 3.3.18 Resistive Voltage Profile as a Function of Time, Case 3

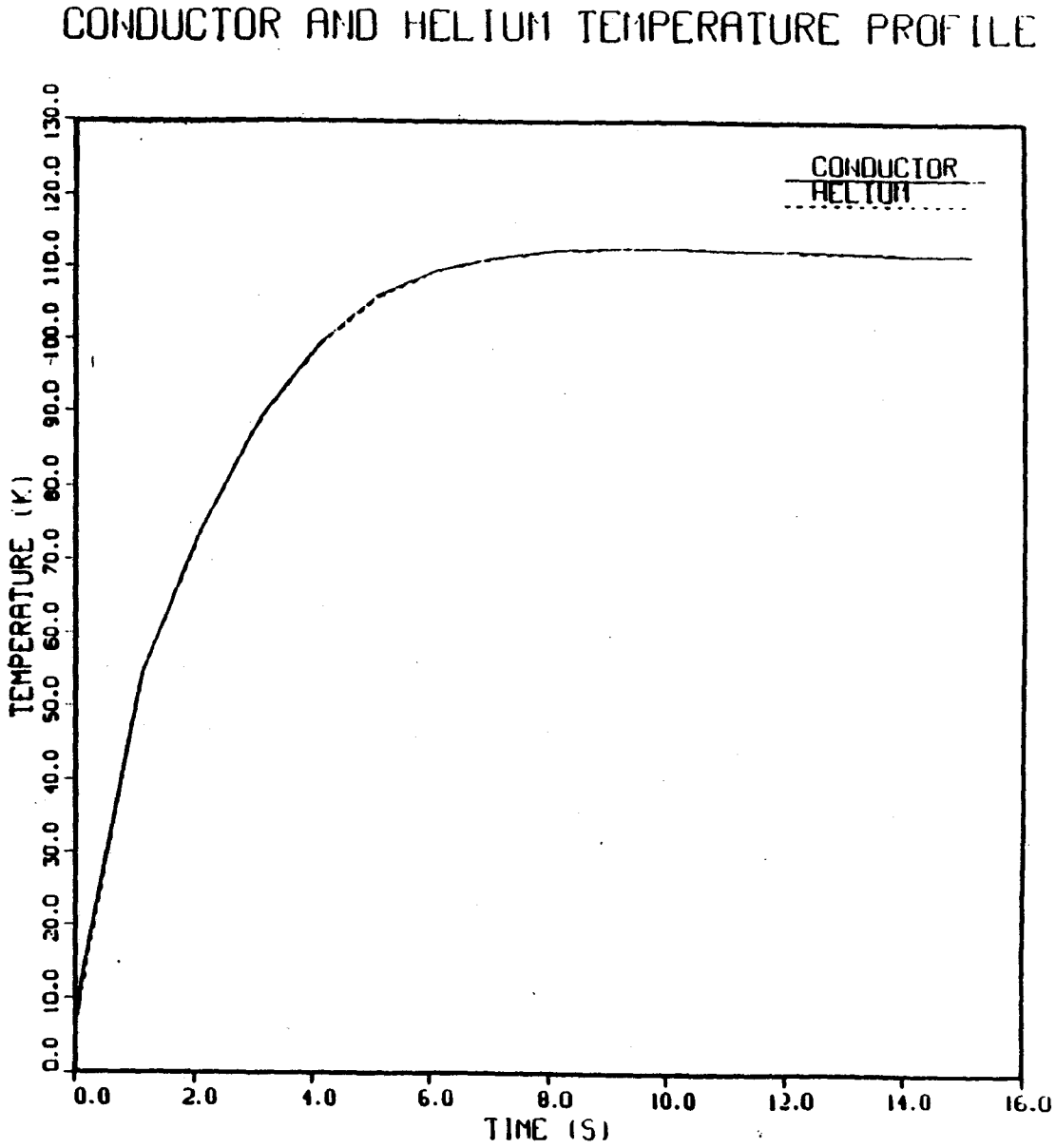

Figure 3.3.19 Conductor and Helium Temperature Profiles at Conductor Center vs Time, Case 3

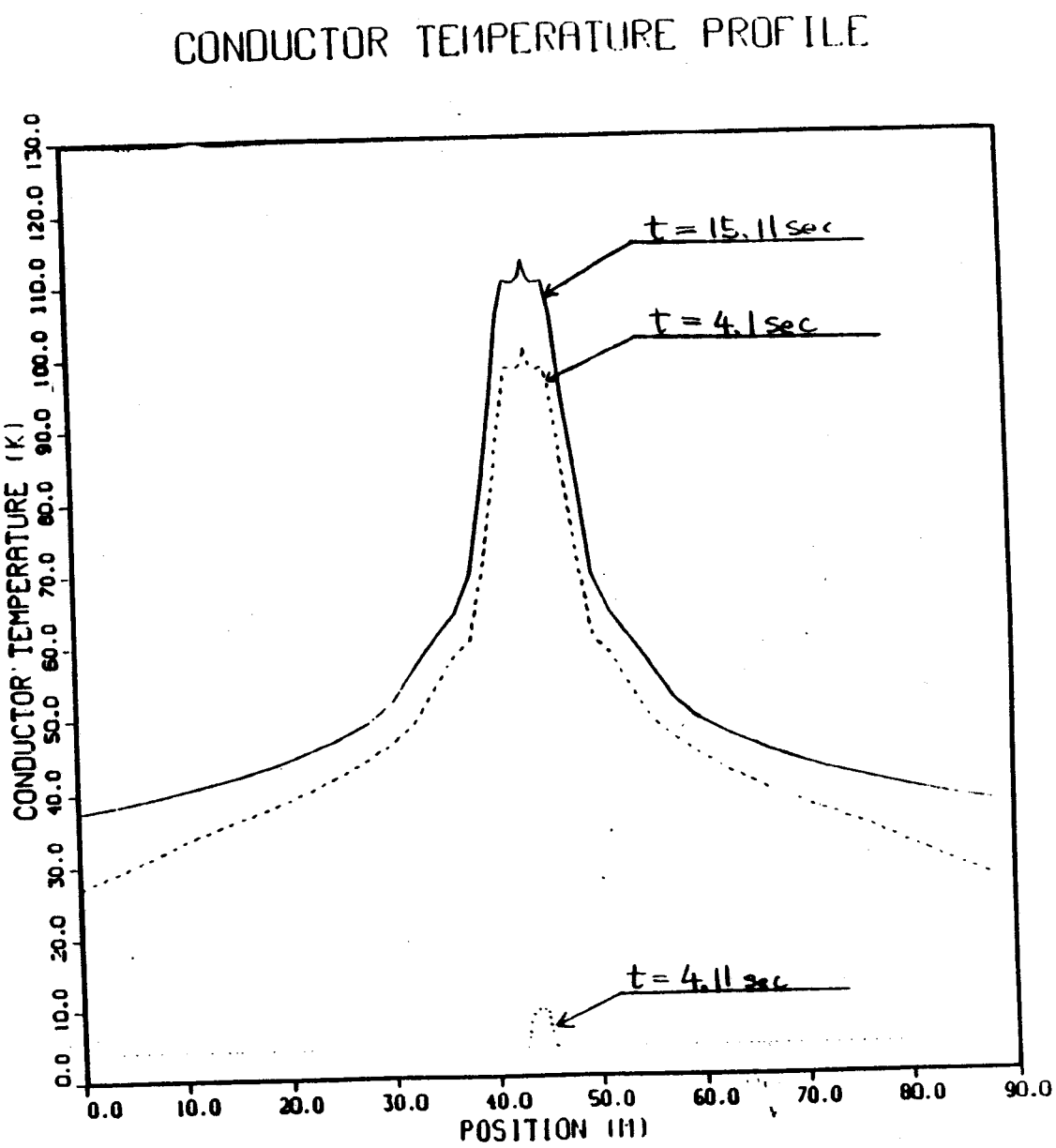

Figure 3.3.20 Conductor Temperature Profile at Three Times vs Position, Case 3

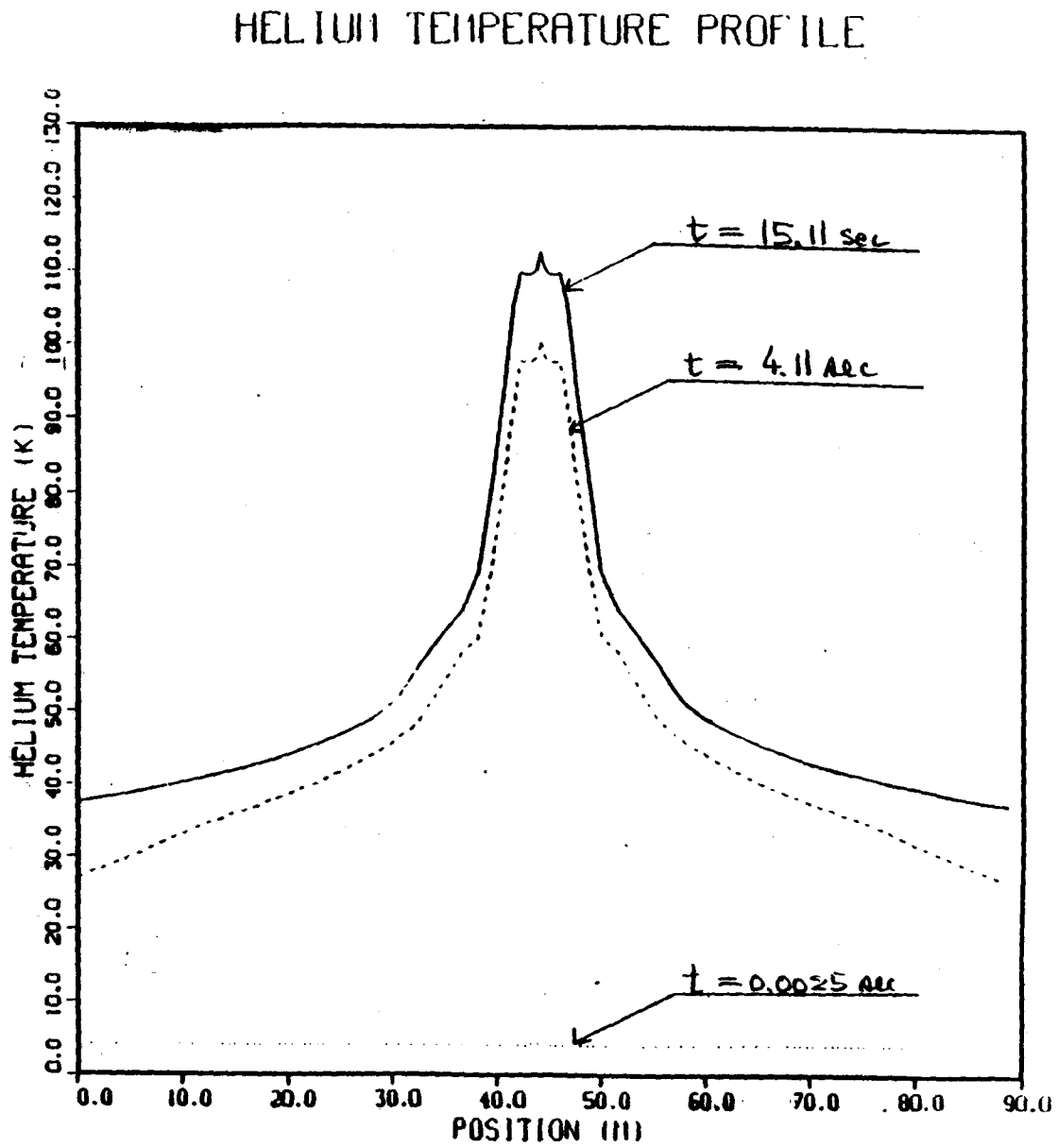

Figure 3.3.21 Helium Temperature Profile at Three Times as a Function of Position, Case 3

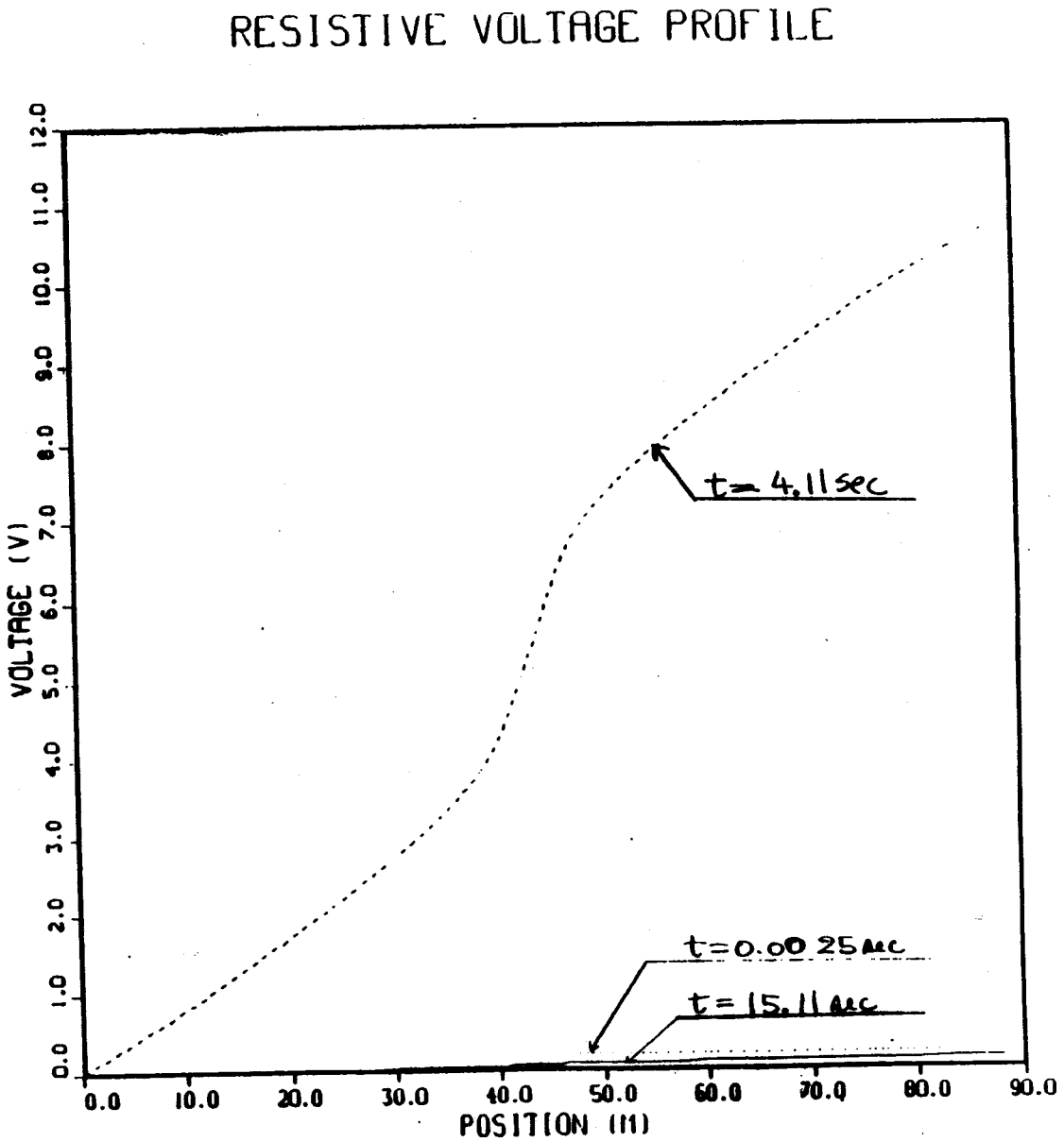

Figure 3.3.22 Resistive Voltage Profile at Three Times vs Position, Case 3

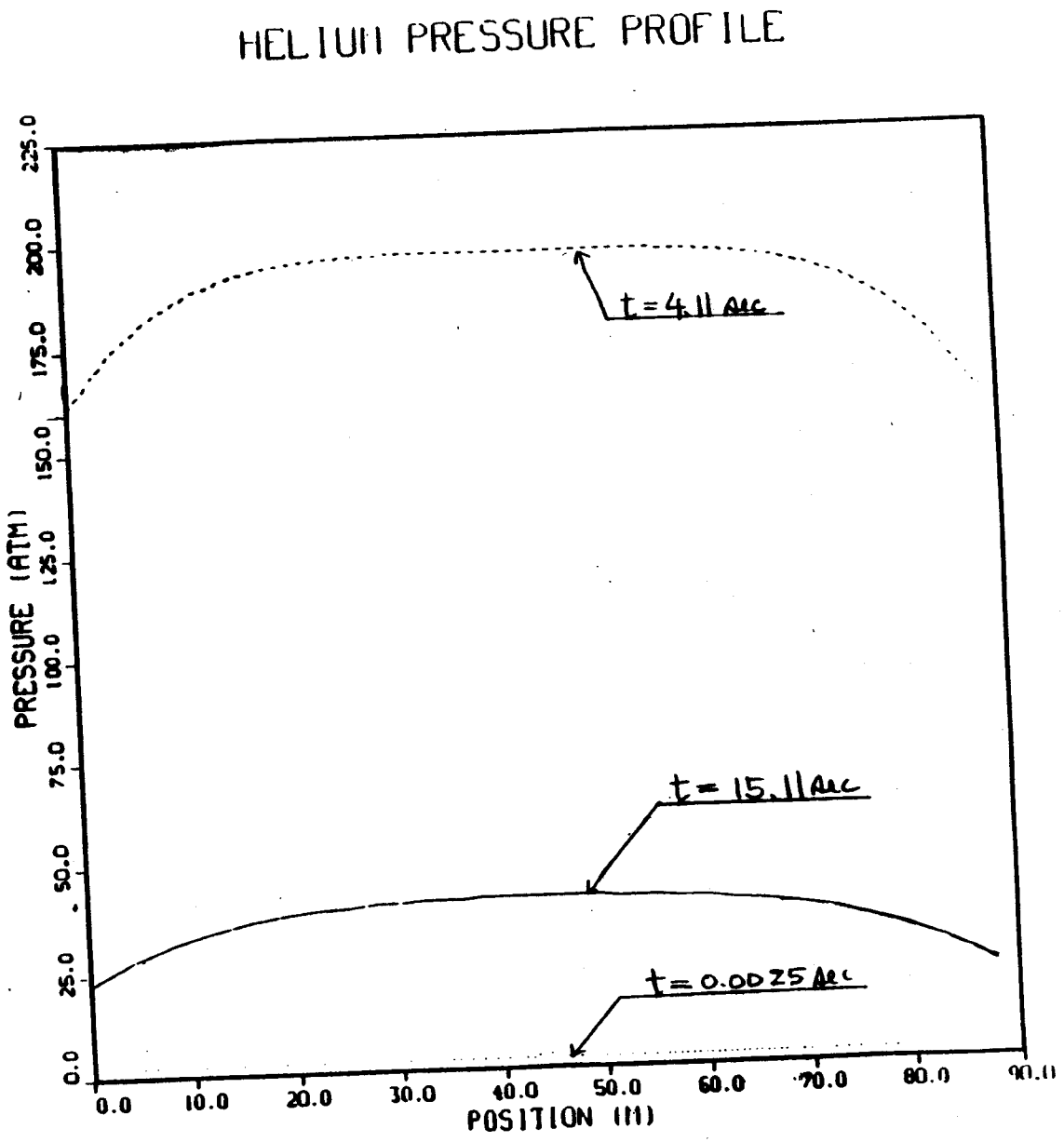

Figure 3.3.23 Helium Pressure Profile at Three Times vs Position, Case 3

3.4 CONCLUSIONS

A computer program developed by V.D. Arp[9] has been modified to analyze recovery and quench propagation in a superconducting coil with and without control of the current decay during a discharge .

Three test cases were designed to examine the performance of the program. Analyses show the characteristic behavior of the conductor for both recovery (Figs. 3.2, 3.3 and 3.6 - 3.9) and nonrecovery.(Figs. 3.12 - 3.15 and 3.19 - 3.22). For the nonrecovery condition, a finite difference form of the circuit equation was introduced into the original code in order to analyze the coil behavior with a discharge circuit. The difference between cases with and without the finite difference form is seen in the current profiles as shown in Figs. 3.3.10 and 3.3.17. This difference in the current profiles affects the resistive voltage behavior as shown in Figs. 3.3.11 and 3.3.15 (recovery), and Figs. 3.3.18 and 3.3.22 (nonrecovery). Operating parameters were chosen arbitrarily to demonstrate both recovery and the nonrecovery behavior, and to examine the effect of coil discharge. The program must now be verified by using a realistic range of operating parameter values.

In the nonrecovery cases, very high pressures (200 atm) were obtained. Since some coolant property correlations become uncertain above 30 atm, the resulting pressure in the nonrecovery cases include the uncertainty. In order to perform a more accurate analysis, it will be necessary to obtain helium property correlations for high pressure and temperature.

This section has emphasized the response of a superconducting coil to temperature and current changes. The effect of the magnetic field is not considered here. As a result, the magnetic field is assumed to be constant under all circumstances. In future studies, the effect of the magnetic field, particularly due to coil discharge, will be introduced into the program.

REFERENCES

[1] D.B.Montgomery,"The Ignition Step:U.S. Experimental Plans and Machines Design Alternatives," IEEE/CH 2251-7/86, pp.19-25(1986).

[2] L.Dresner,"Protection Consideration for Force-Cooled Superconductors," IEEE/CH 2251-7/86, pp.1218-1222(1986).

[3] S.R.Shanfield, "Transient Cooling in Internally Cooled Superconductors," Ph.D thesis, Nuclear Engineering Department, MIT(1981).

[4] L.Dresner, "Stability of Internally Cooled Superconductors: A Review," *Cryogenics*, October, pp.558-563(1980).

[5] M.V.Ricci and L.Bottura, "About the Necessity of a 3-D Code for Quench Calculations," NET/88/TE/100-S-03(1988).

[6] J.Mivervini and L.Bottura, "Stability Analysis of NET TF and PF Conductors," EUR/FU-XII/80/87/77(1987).

[7] L.Bottura, "Transient Thermal Analysis of the NET-TF Coil," NET/IN/87-056(1987).

[8] G.Krafft and G.Zahn, "Experimental and Theoretical Investigation of Heat-Induced Transients in Forced-Flow Helium Cooling System," Symposium of Fusion Engineering, IEEE CH1441-5/79, pp.1724-1728(1979).

[9] V.D.Arp, "Stability and Thermal Quenches in Force-Cooled Superconducting Cables", 1980 Superconducting MHD Magnet Design Conference, MIT, pp.142-157(1980).

[10] Z.J.J.Stekly and R.J. Thome, "Lightweight Superconducting MHD Magnets," AFAL-TR-72-32, Vol.1(1972).

[11] R.J.Thome, "Magnet Power Supplies and Protection," Lecture Notes, Summer Course ; Superconducting Magnet Design(1981).

APPENDIX I.

Nomenclature

Symbol	Definition	Units
A	Flow Cross Section	m^2
A_{cu}	Copper Cross Section	m^2
C	Sound Velocity	m/s
C_p	Specific Heat of Conductor	$J/kg \cdot K$
D	Hydraulic Diameter ($= 4A/P_h$)	m
f_a	Fanning Friction Factor	—
F	$(P_f/2A)\, v\, \lvert v \rvert\, f_a$	J/m^3
h	Local Instantaneous Heat Transfer Coefficient	
H	Fluid Enthalpy	J/kg
I	Current	A
I_o	Initial Current	A
k	Thermal Conductivity of Conductor	$W/m \cdot K$
l	Total Length of Conductor	m
$l1$	Start of Heated Region	m
$l2$	End of Heated Region	m
l_n	Length of Normal Region of Conductor	m
L	Coil Inductance	H
n	Number of Time Increments	
P, P_o	Pressure	Pa
P_f	Hydraulic Perimeter (Flow Perimeter)	m
P_h	Inital Input Energy / Mass of Conductor	J/kg

Symbol	Definition	Units
P_h	Heated Perimeter of Conductor	m
Q_n	Conductor to Helium Heat Flux	W/m
Q_j	Joule Heating Rate in Conductor	W/m
Q_o	Initial Perturbation Heating Rate in the Conductor	W/m
R	Resistance of Propagating Normal Region	Ω
R_d	Resistance of Dump Resistor	Ω
T_c	Critical Temperature	K
T_{cs}	Critical Current Sharing Temperature	K
T_h	Helium Temperature	K
T_w	Wall Temperature	K
t	Time	s
Δt	Length of Time Increments	s
Δt_h	Heat Pulse Length	s
v	Fluid Velocity	m/s
V_R	Resistive Voltage	V
w	Transition Heated Region Length	m
x	Length Coordinate (Parallel to the Conductor)	m
ϕ	Potential Function Whose Gradient Gives Body Forces on the Fluid	J/kg
ρ	Resistivity of Conductor	Ω-m
ρ^*	Fluid Density	kg/m³
ρ'	Conductor Density	kg/m²

APPENDIX II – (1)

Input Data of SCAN Code

Variables	Definition	Data
lnth	total length of conductor	88 m
lnth 1	start of heated region, excluding transition region	43 m
lnth 2	end of heated region, excluding transition region	45 m
width	transition region length	0.5 m
amps	operating initial current	25000 A
bss	steady state background magnetic field	9.0 T.
btro	initial transient field decay with magnet current	0.0 T.
enrg kg	total energy deposited in conductor during heat pulse	see (1)
httime	heat pulse time	1.0×10^{-2}
no1	number of nodes before heated region	19
n12	number of nodes in heated region	18
nint	total number of nodes (> no1+n12)	50
notest	=0 integration is stopped if thermal runaway or recovery detected	
	=1 integration continues until time limit reached	1
thmax	maximum helium temperature	300 K
pamax	maximum helium pressure	200 Pa
twmax	maximum conductor temperature	300 K
tzero	initial temperature	4.2 K

Variables	Definition	Data
Valve 1	Valve = 0; Constant pressure boundary	10000
Valve 2	Valve > 100 Constant flow boundary	10000
Vel	Velocity of supercritical helium	0.0 m/s
dtime 1	time steps for three time regions	2.5×10^{-3} s
dtime 2		5.0×10^{-2} s
dtime 3		1.0 s
pin	inlet reservoir pressure.	2.4×10^{5} Pa
eps 1	relative error for integration in each time region	5.0×10^{-4}
eps 2		2.0×10^{-3}
eps 3		8.0×10^{-3}
time 1	end time for each time region	1.0×10^{-2} s
time 2		0.1 s
timemx		15 s
damp	damping term coefficient.	5
dampx	maximum value of the damping term	1000
axf	cross sectional area of fluid	9.889×10^{-5} m^2
axm	cross sectional area of conductor	1.838×10^{-4} m^2
perimf	wetted perimeter	1.137 m
perimh	~~wetted~~ heated perimeter.	1.069 m
ninput	boundary condition flag :	
	= 1 initial velocity (vel) specified	1
	= 2 initial outlet pressure (pout) specified	

Variables	Definition	Data
idsc	superconductor type	
	= 0 Copper	
	= 1 NbTi	
	= 2 Nb_3Sn	2.
dktime	decay time constant for external time decay	3.0
reactm	reaction time constant for external time decay	15.0
cusc	copper to non-copper volume ratio	1.7
rrr	residual resistance ratio of copper matrix	75
dinduc	coil inductance	See (1)
drex	resistance of dump resistor	See (2).

APPENDIX II -(2)

Operating Conditions for Cases 1, 2 and 3

	Case 1	Case 2	Case 3
enrg kg	20 J/kg	60 J/kg	60 J/kg
dinduc	0.0 H	0.0 H	5.0×10^{-2} H
drex	0.0 Ω	0.0 Ω	5.0×10^{-2} Ω

APPENDIX II-(3)

Output Data of Scan Code

Variables	Definition	Units
patm	Helium pressure	atm
dPdx	dP/dx	atm/m
efield	Electric Field	V/m
tfluid	Helium temperature	°K
twall	Wall temperature	°K
qmsec	Mass flow rate	g/sec
lamda	Heat transfered from conductor to coolant	W
heat	Net power input to conductor	W
htcoef	Heat transfer coefficient	W/m².K
bfield	Magnetic field	T
dkamp	Current	A
volt	Voltage	V
res	Resistance	Ω
denmet	Metal density	Kg/m³
kond	Thermal conductivity	W/m.K
dkdt	dk/dt	W/m.K²
cpwall	Specific heat	J/kg.K
rho	Resistivity at 0 T of magnetic field	Ω-m
rf	Ratio of resistivity at bT to resistivity at 0T	

APPENDIX III - (1)

Simplified flow chart showing major component

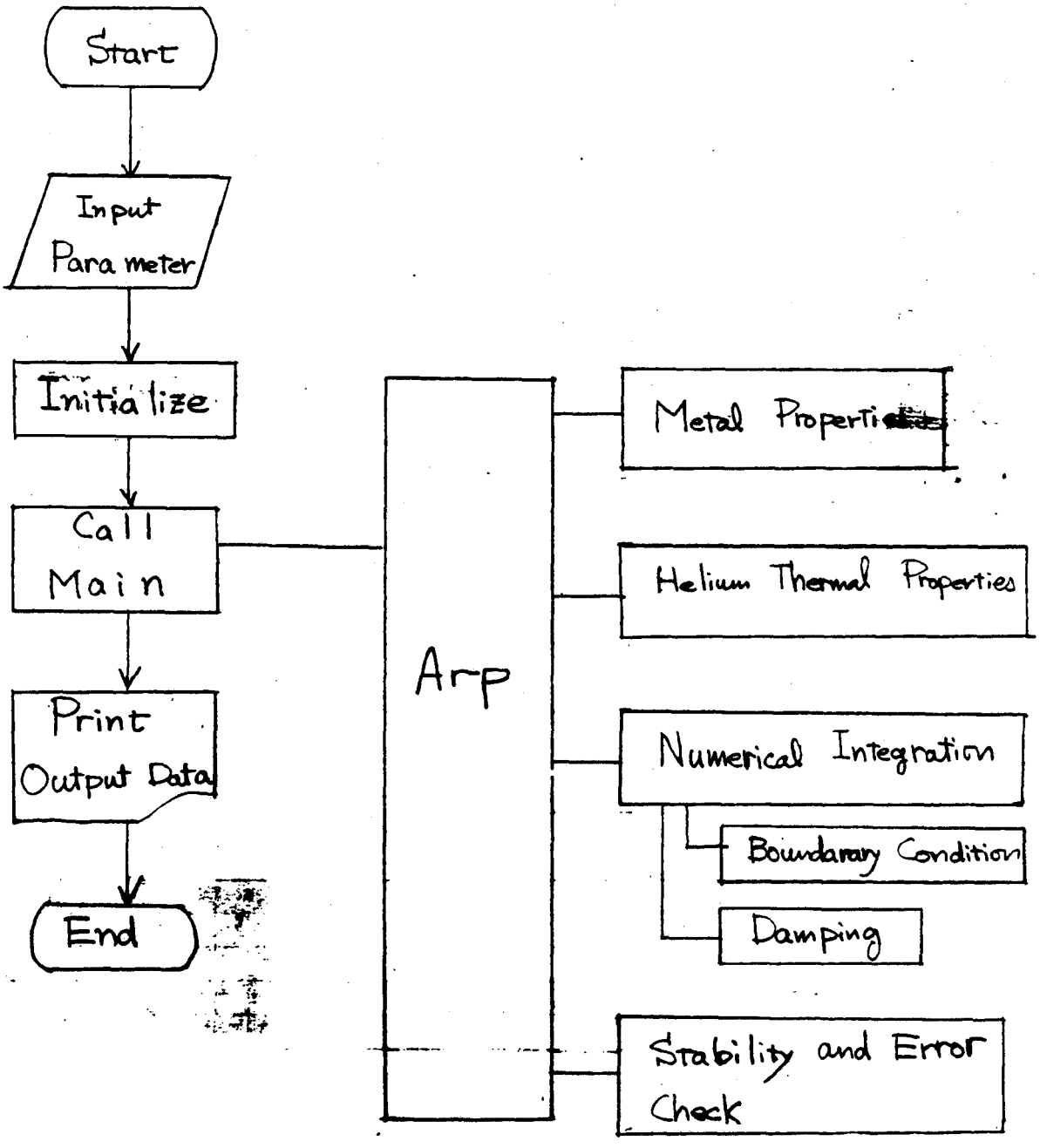

APPENDIX III - (2)

Important Subroutine in Scan code

Main — Arp : actual numerical calculation

- idSC=0 — Metal : calculation of bare copper conductor properties
  - =1 — $NbTi$: calculation of $NbTi$ superconductor properties
  - =2 — Nb_3Sn : calculation of Nb_3Sn superconductor properties
- Start : calculation of initial conditions
- Grid : determination of the node spacing of the conductor
- Pdecol : numerical integration pachage (solve the non-linear partial differential equations)
- Values : Compatation of u and $\frac{dy}{dx}$ at each node
- Props : calculation of coolant and conductor properties, friction factor and heat transfer coefficient
- Figure : graphic plotter routine of result.